Synthesis of MWCNTs by Chemical Vapor Deposition from Methane Using FeMo/MgO

catalyst : Role of Hydrogen and Kinetic Study

Mr. Chawalkul Chotmunkhongsin

A Thesis Submitted in Partial Fulfillment of the Requirements

for the Degree of Master of Engineering in Chemical Engineering

Department of Chemical Engineering

FACULTY OF ENGINEERING

Chulalongkorn University

Academic Year 2020

การสังเคราะห์ท่อนาโนคาร์บอนชนิดผนังหลายชั้นโดยกระบวนการตกสะสมไอสารเคมีจากมีเทนด้วย
ตัวเร่งปฏิกิริยา FeMo/MgO : บทบาทของไฮโดรเจน และการศึกษาจลนพลศาสตร์

นายชวาลกูล โชติมั่นคงสิน

วิทยานิพนธ์นี้เป็นส่วนหนึ่งของการศึกษาตามหลักสูตรปริญญาวิศวกรรมศาสตรมหาบัณฑิต
สาขาวิชาวิศวกรรมเคมี ภาควิชาวิศวกรรมเคมี
คณะวิศวกรรมศาสตร์ จุฬาลงกรณ์มหาวิทยาลัย
ปีการศึกษา 2563

Thesis Title	Synthesis of MWCNTs by Chemical Vapor Deposition from Methane Using FeMo/MgO catalyst : Role of Hydrogen and Kinetic Study
By	Mr. Chawalkul Chotmunkhongsin
Field of Study	Chemical Engineering
Thesis Advisor	Assistant Professor Dr. APINAN SOOTTITANTAWAT
Thesis Co Advisor	Dr. Sakhon Ratchahat

Accepted by the FACULTY OF ENGINEERING, Chulalongkorn University in Partial Fulfillment of the Requirement for the Master of Engineering

.... Dean of the FACULTY OF ENGINEERING
(Professor Dr. SUPOT TEACHAVORASINSKUN)

THESIS COMMITTEE

.... Chairman
(Professor Dr. MUENDUEN PHISALAPHONG)

.... Thesis Advisor
(Assistant Professor Dr. APINAN SOOTTITANTAWAT)

.... Thesis Co-Advisor
(Dr. Sakhon Ratchahat)

.... Examiner
(Professor Dr. TAWATCHAI CHARINPANITKUL)

.... External Examiner
(Assistant Professor Dr. Weerawut Chaiwat)

ชวาลกูล โชติมั่นคงสิน : การสังเคราะห์ท่อนาโนคาร์บอนชนิดผนังหลายชั้นโดยกระบวนการตก
สะสมไอสารเคมีจากมีเทนด้วยตัวเร่งปฏิกิริยา FeMo/MgO : บทบาทของไฮโดรเจน และ
การศึกษาจลนพลศาสตร์. (Synthesis of MWCNTs by Chemical Vapor Deposition
from Methane Using FeMo/MgO catalyst : Role of Hydrogen and Kinetic Study)
อ.ที่ปรึกษาหลัก : ผศ. ดร.อภินันท์ สุทธิธารธวัช, อ.ที่ปรึกษาร่วม : อ. ดร.สาคร ราชหาด

ท่อนาโนคาร์บอน (CNTs) ถูกสังเคราะห์โดยการตกสะสมไอสารเคมี (CCVD) จากมีเทนด้วย
ตัวเร่งปฏิกิริยา FeMo/MgO ในเครื่องปฏิกรณ์แบบเบดนิ่ง ในงานวิจัยนี้ทำการศึกษาบทบาทของ
ไฮโดรเจน และจลนพลศาสตร์ต่อกระบวนการสังเคราะห์ CNTs โดยเปรียบเทียบกระบวนการการใช้
ไฮโดรเจนวิธีต่างๆ คือ การใช้ไฮโดรเจนรีดิวซ์ตัวเร่งปฏิกิริยา และการป้อนไฮโดรเจนระหว่างการก่อตัว
ของ CNTs โดยจากการศึกษาพบว่าบทบาทที่สำคัญของไฮโดรเจนต่อกระบวนการสังเคราะห์ CNTs คือ
การเปลี่ยนแปลงโครงสร้างของตัวเร่งปฏิกิริยา FeMo/MgO ในกระบวนการรีดิวซ์ตัวเร่งปฏิกิริยาที่จะ
เปลี่ยนโครงสร้างของตัวเร่งปฏิกิริยาเป็นโลหะ FeMo (metallic) ทำให้ได้ปริมาณผลได้สูงกว่าตัวเร่ง
ปฏิกิริยาที่ไม่ผ่านกระบวนการรีดิวซ์ ถึง 5 เท่า แต่จะมีขนาดเส้นผ่านศูนย์กลางที่ใหญ่กว่าและสัดส่วน
ความเป็นผลึกต่ำกว่า CNTs จากตัวเร่งปฏิกิริยาที่ไม่รีดิวซ์ที่จะอยู่ในโครงสร้างของ Mo_2C อยู่เล็กน้อย
การเติมไฮโดรเจนระหว่างการสังเคราะห์ CNTs ในสัดส่วนที่เหมาะสมสามารถช่วยเพิ่มปริมาณผลได้ขึ้น
เล็กน้อย แต่หากมีปริมาณไฮโดรเจนมากเกินไปจะขัดขวางการเปลี่ยนของมีเทนและเกิดผลิตภัณฑ์น้อยลง
ปฏิกิริยาไฮโดรจีเนชัน (hydrogenation) สามารถเกิดระหว่างการก่อตัวของ CNTs โดยใช้คาร์บอนเป็น
สารตั้งต้น ไฮโดรจีเนชันไม่เลือกเกิดกับอัญรูปใดอัญรูปหนึ่งของคาร์บอน ดังนั้นการเติมไฮโดรเจนจะไม่
ช่วยรักษาเสถียรภาพของตัวเร่งปฏิกิริยาจากการกำจัดอสัณฐานคาร์บอนออกจากผิวของตัวเร่งปฏิกิริยา
และไม่เพิ่มสัดส่วนความเป็นผลึกให้กับผลิตภัณฑ์อีกด้วย การศึกษาจลนพลศาสตร์ของการสังเคราะห์
CNTs สอดคล้องกับสมการอันดับหนึ่งเทียมของความดันย่อยมีเทน โดยอัตราการก่อตัวของ CNTs จะ
เพิ่มขึ้นตามความดันย่อยของมีเทนและจะลดลงเมื่อเกินระดับอิ่มตัว ค่าพลังงานก่อกัมมันต์มีค่าเท่ากับ
13.22 กิโลจูลต่อโมลทำให้ขั้นการควบคุมอัตราปฏิกิริยา (rate controlling step) อาจอยู่ในช่วงการถูก
ควบคุมด้วยการถ่ายโอนมวลสาร

สาขาวิชา	วิศวกรรมเคมี	ลายมือชื่อนิสิต ....
ปีการศึกษา	2563	ลายมือชื่อ อ.ที่ปรึกษาหลัก ....
		ลายมือชื่อ อ.ที่ปรึกษาร่วม ....

6270060521 : MAJOR CHEMICAL ENGINEERING

KEYWORD: Synthesis of CNTs, CNTs, kinetic study, Hydrogen, Catalytic Chemical Vapor Deposition

Chawalkul Chotmunkhongsin : Synthesis of MWCNTs by Chemical Vapor Deposition from Methane Using FeMo/MgO catalyst : Role of Hydrogen and Kinetic Study . Advisor: Asst. Prof. Dr. APINAN SOOTTITANTAWAT Co-advisor: Dr. Sakhon Ratchahat

In this study, carbon nanotubes (CNTs) were synthesized by chemical vapor deposition (CCVD) of methane over FeMo/MgO catalyst in a fixed-bed reactor. The role of hydrogen on CNTs synthesis and kinetics of CNTs formation were experimentally investigated. The study revealed that hydrogen in the catalyst reduction process plays an important role in the structural changes of FeMo/MgO catalyst. The catalyst structure fully transformed into metallic FeMo, resulting in the increased yield of 5 folds higher than the non-reduced catalyst. However, the slightly larger diameter and lower crystallinity ratio of CNTs was obtained. The hydrogen co-feeding during the synthesis can slightly increase the CNTs yield, achieving the optimum amount of hydrogen addition. Further increase in hydrogen to the excess condition would inhibit the methane decomposition, resulting in less product yield. It was found hydrogenation of carbon to methane has proceeded during hydrogen co-feed process. However, the hydrogenation was non-selective to allotropes of carbon. Therefore, the addition of hydrogen would not benefit either maintaining the catalyst stability or improving the crystallinity ratio of the product by eliminating amorphous carbon from the catalyst surface and the product. The kinetic model of CNTs formation correlates with pseudo-first order of methane partial pressure. The rate of CNTs formation increases with the partial pressure of methane but decreases when saturation is exceeded. The activation energy was found to be 13.22 kJ mol^{-1}, showing the rate controlling step to be in the process of mass transfer.

Field of Study:	Chemical Engineering	Student's Signature	....
Academic Year:	2020	Advisor's Signature	....
		Co-advisor's Signature	....

ACKNOWLEDGEMENTS

TABLE OF CONTENTS

LIST OF TABLES

LIST OF FIGURES

จุฬาลงกรณ์มหาวิทยาลัย

CHULALONGKORN UNIVERSITY

Chapter 1

Introduction

1.1 Background

Carbon-Nanotubes (CNTs) were discovered over 3rd decade ago in 1991 [1] ; its unique chemical and physical properties have been researched and applied in many applications such as semi-conductor, battery, reinforced material and universal composited material [2]. The synthesis of CNTs can be as simple as the presence of a carbon-based substrate under suitable conditions that is allowing a variety of CNTs to be directly synthesized as a product and also be by-product in other process, such as hydrogen production. The catalytic decomposition of methane gas to produce hydrogen gas and by-product, carbon formed on the catalyst surface [3-6]. From above, H_2 gas generally found during CNTs synthesis. There are many researched show that all of these process success to produce a CNTs, which are H_2 free process [7], H_2 was used only to pre-reduction of catalyst process but not to CNTs formation process [8], or H_2 was used in the entire process from reduction of catalyst to synthesis of CNTs process [9, 10].

The study of H_2 roles or effect of H_2 to CNTs production has been studied for a long time. The research of Piedigrosso et al.[11] reported H_2 caused hydrogenation that eliminated both of CNTs and amorphous carbon, from these report other research found that, the used of H_2 during CNTs synthesis increased yield of CNTs [12-18] because H_2 etched amorphous carbon out from catalyst surface that kept reaction still occur. The other effect of H_2 was widely reported, which is the H_2 concentration made different CNTs diameter [14, 15, 18] included effect to formation of SWCNTs some researcher found H_2 hinder formation of SWCNTs [19],[20]. On the other hand, the H_2-free or less concentration of H_2 process could not synthesis a SWCNTs [21], including to MWCNTs [22]. The reason of this effect was reported in the same way, H_2 has a roles to control the size, phase, and morphology of catalysts. For CNTs synthesis, catalyst is the one necessary factor to control CNTs formation, such as the same Fe-

based catalyst but one is α-Fe phase and other one is Fe_3C phase, the formation of CNTs occur with a huge different in yield, diameter and CNT characteristic. He et al. [23] and Torres et al. [6] reported Fe_3C phase resulting in the synthesis of Bamboo like CNTs, additionally Fe_3C forming smaller diameter CNTs but less yield than α-Fe [12, 24]. Research has shown that the addition of Mo can increase the efficiency of CNTs synthesis by increasing yield and enhancing better stability at high temperatures [25],[8]. Furthermore, mechanisms of the effects of hydrogen on the synthesis of CNTs using FeMo/MgO as a catalyst have not been reported.

Finally, the production of CNTs has deeply developed that directly affecting to the continued decline in sales prices and expected that the price will further go down globally [26], even so CNTs are still expensive, approximately price of SWCNTs and MWCNTs are 38,000฿ [27] and 3,400฿ [28] per gram, respectively. The market for MWCNTs has a decline in large-scale production; however, there still remains global demand of >2000-2500 tons per annum with increased demand in composites, automotive and aerospace applications and especially as battery additives in Asia [29]. In contrast, H_2 demand is increasing consistently. Therefore to compete in the CNTs market, manufacturers should balance costs to suit the CNTs properties.

Consequently, this work focuses on studying the role of H_2 to whole process of CNTs synthesis by using FeMo/MgO as a catalyst and finding out in-depth behavior of each process to guide further improvements in CNTs manufacturing process as well as its reaction kinetic.

1.2 Objectives

1. Study H_2 roles for synthesis of CNTs in both of reduction phase and formation of CNTs phase as well as its reaction kinetic.

1.3 Scopes of research

1. Carbon nanotube (CNTs) were synthesized by catalytic chemical vapor deposition method (CCVD) of methane on FeMo/MgO catalyst in fixed-bed reactor.

2. The CCVD method was conducted under atmospheric pressure, N_2 was used as a carrier gas to adjust the total gas flow rate equal to 200 standard cubic centimeters per minute (SCCM), and 0.5 g catalyst was used per experimental.

3. Designated 4 process to study roles of CNTs which are H_2-free process (nR-woH$_2$), H_2 co-feed process (nR-wH$_2$), H_2 pre-reduction of catalysts (R-woH$_2$) and H_2 combined process (R-wH$_2$)

4. Effect of H_2 concentration was investigated by using H_2 co-feed process with varied CH_4:H_2 ratio

5. Hydrogenation reaction was investigated through; catalyst stability and the reaction of as-prepared CNTs in H_2 atmosphere.

6. The reaction kinetics of CNTs synthesis will be investigated in term of product yield rate.

Chapter 2

Literature Reviews

2.1 Carbon Nanotubes

Carbon Nanotubes is the 1-dimensional nano-materials, forming by rolled-up of graphene sheet layer, made to number of CNTs wall such as Single-walled (SWCNTs), Double-walled (DWCNTs), or Multi-walled CNTs (MWCNTs). CNTs nano-structure were arranged in pattern from chemically bonded with sp^2 bonds [30] that made less defect of structure and give an unique physical and chemical properties. CNTs have been researched and applied in many applications such as semi-conductor, battery, reinforced material and universal composited material [2].
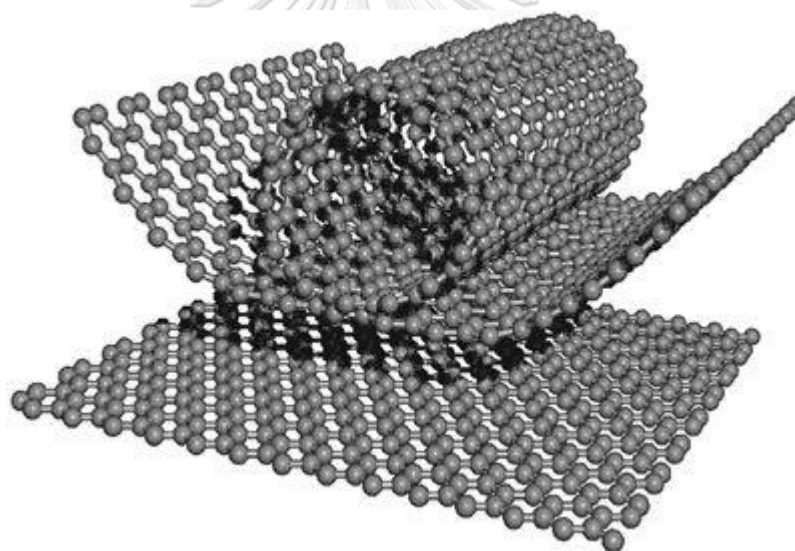
Figure 2. 1 Schematic of how graphene could roll up to form a carbon nanotube. [30]

2.2 Synthesis of CNTs method

CNTs can synthesize in varied way. Firstly lijima [1] was discovered CNTs by Arc discharge method, after that synthesis of CNTs was continuously developed and found as follows.

2.2.1 Arc discharge

Arc discharge invented in 1991 by Iijima [1], by using electricity and electrodes to evaporate carbon and rearrange its structure under a controlled atmosphere. (Eg, containing methane and argon) formed into SWCNTs. Figure 2.2 shows an apparatus used in the synthesis of CNTs by Arc discharge. The electrodes used must be carbon rods such as graphite. [31]
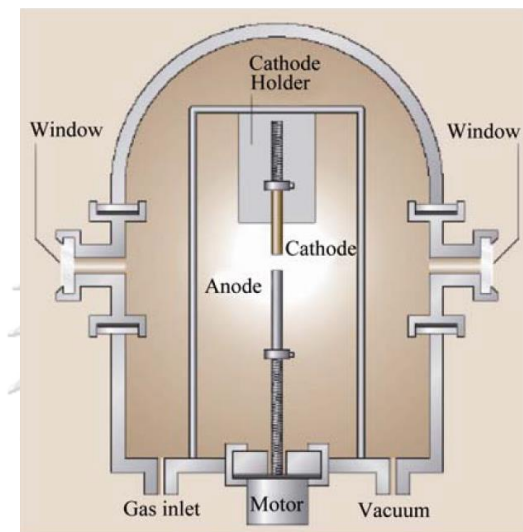
Figure 2. 2 Synthesis of CNTs by Arc discharge method [31]

2.2.2 High pressure carbon monoxide reaction (HiPCO®)

The process was developed by Rice University in 1999 as a furnace synthesis. Where the reactants and catalysts are both in a gas phase. The catalyst used is $Fe(CO)_5$ and the precursor is carbon monoxide (CO). This process is suitable for industrial scale production as the produced CNTs are free to form. It does not bonded to the catalyst like the CVD method and can be operated continuously. [31]

2.2.3 CoMoCAT® Process

This process was developed at the University of Oklahoma using Cobalt and Molybdenum as a catalyst and using CO as a substrate at 700-950 °C. It can provide high throughput and can be extended to industrial scale production. This method are widely used to produce large-capacity CNTs.

2.2.4 Catalytic chemical vapor deposition (CCVD)

CCVD process is a highly recommend and widely used method for producing CNTs, because of uncomplicated, highly flexibility and scalable process. This method use catalyst placed inside a tubular reactor with high temperature (600-1200 $^{\circ}$C), then hydrocarbon gases/liquid (vapor) such as methane, ethylene and other process gas such as nitrogen, argon or hydrogen were feed into the tubular reactor. The product CNTs will form on catalyst surface [32]. CCVD is highly flexibility because, this method can be adapt in many ways such as the used of floating catalyst (ferrocene) [33], VACNTs which used catalyst coated on substrate such as silicon wafers [34] or used to be a prototype to develop fluidized bed reactor.
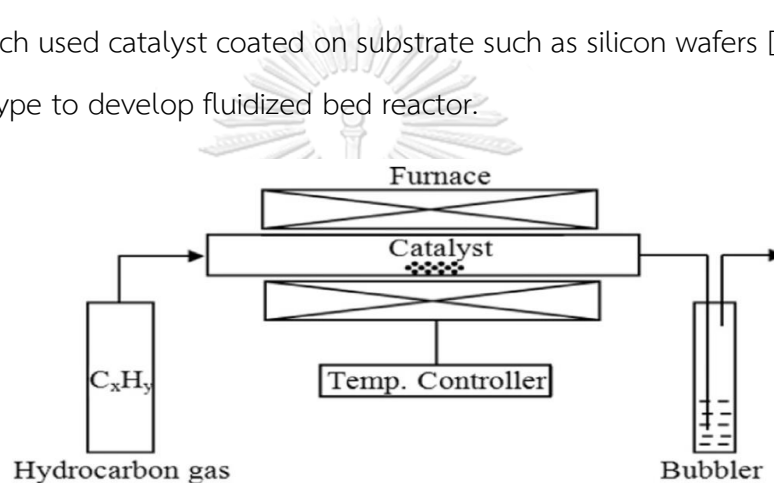
Figure 2. 3 Schematic diagram of CCVD method [32]

2.3 Catalysts for synthesis of CNTs by CCVD method

The key factor to synthesis CNTs by CCVD method is catalysts. The common catalysts generally used in CNTs synthesis can be mono-metallic such as metals Fe, Ni, Co on various supporting materials such as Al_2O_3, SiO_2 and MgO [35]. Researched of Molybdemun (Mo) was introduced, which has a relatively low efficiency in the synthesis of CNTs compared to iron, nickel and cobalt but when Mo was mixed with other metals, it was bimetallic catalysts. For example, FeMo, NiMo, or CoMo found that Mo improves the catalyst activity in the synthesis of CNTs, with Mo act as a promoter to help better disperse atoms of other metals [25], increase the solubility of the carbon atoms on the surface of the metal that made higher yield [36]. In addition,

these bimetallic catalysts tend to have good stability at higher temperatures than mono-metallic catalysts. Thus, the high metal dispersion of the catalyst can be maintained while the formation of SWCNTs at high temperature [8]. The size of the catalyst can be controlled by controlling the metal loading, which are often pre-determined in the preparation of the catalyst. Modification of the catalyst's metal loading has a direct effect on the metal size the metal dispersion [37]. The catalyst support is also important to the CNTs synthesis process. A good supported for the synthesis of CNTs should have typical properties of the supported materials, such as having a high surface area, high porosity, and not catalytic toxicity, or cause a side reaction. In addition, Awadallah [38] et al. has also shown that supported also influence the formation of CNTs. The formation mechanism of CNTs on catalysts are extensively studied and the accepted mechanism is proposed as two types: tip growth and base growth. In general, the bond between the catalyst and the supported (metal-support interaction) characterizes the mechanism.

Xu et al. [39] reported XRD analysis results of calcined Fe, Mo, and FeMo on MgO supported exhibited the diffraction peaks of MgO impregnated with iron and molybdenum, found that no interaction between iron and molybdenum as shown in Fig 2.4.
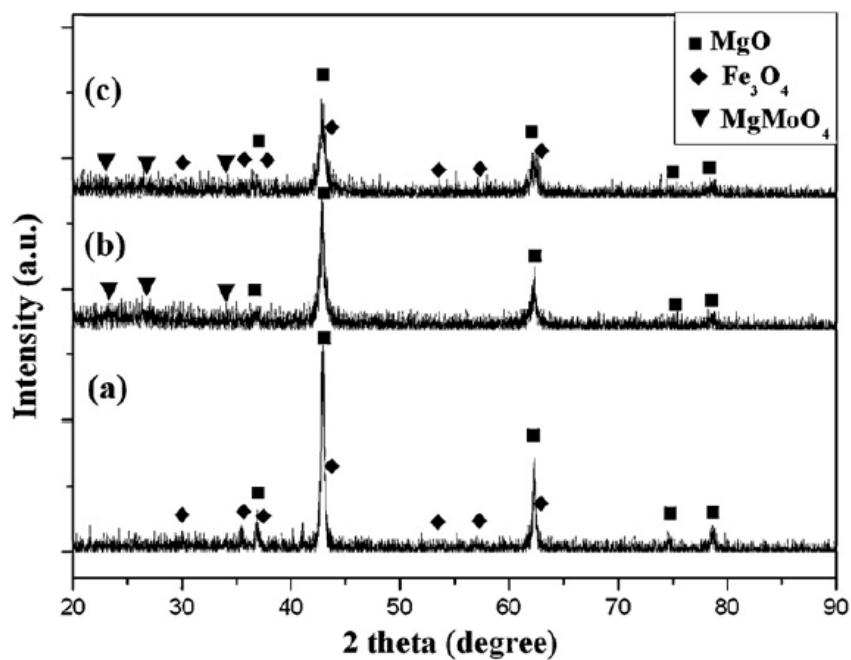
Figure 2. 4 XRD patterns of the catalysts before reduction by hydrogen.
(a)$Fe_{0.1}Mg_2O_{2.15}$, (b) $Mo_{0.1}Mg_2O_{2.3}$, and (c) $Fe_{0.1}Mo_{0.1}Mg_2O_{2.45}$ [39].

The H_2-temperature programmed reduction (H_2-TPR) analysis was used to investigate reducibility of the fresh catalysts. Torres D. et al. [3] reported the reducibility of FeMo/MgO catalyst, found that adding of Mo effects to shifted temperature range from FeMo(0)/MgO, as shown in Fig 2.5
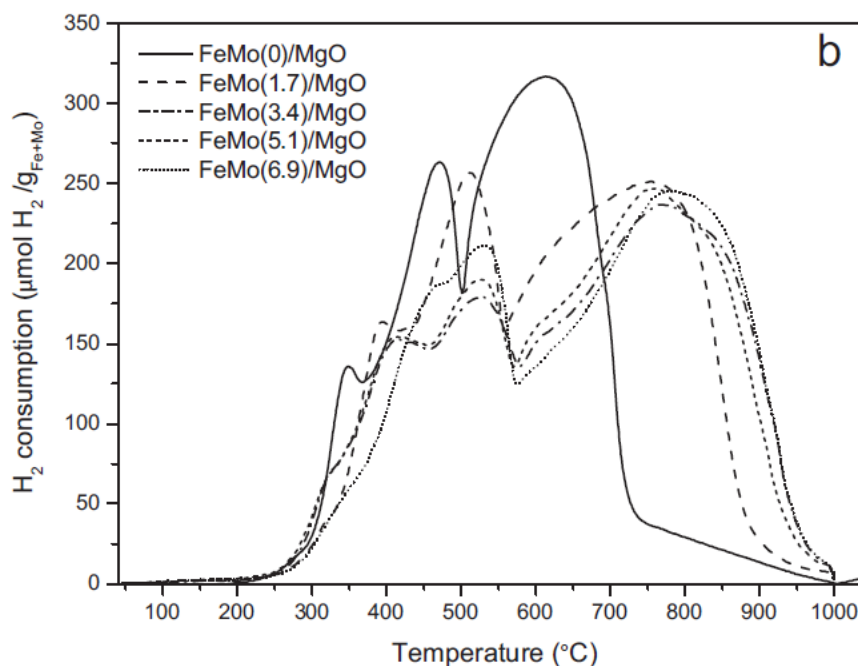
Figure 2. 5 TPR profiles of the fresh calcined catalysts FeMo(X)/MgO [3].

2.4 The formation mechanism of CNTs

Synthesis of CNTs via CCVD method, CNTs formed at the surface of active metal catalyst, so the particle size of the catalyst (active phase) will determined the type of CNTs or the number of wall layers of carbon nanotubes (SWCNTs or MWCNTs) [40]. The formation mechanism of CNTs is shown in Figure 2.6, ie CNTs form at the metal surface determined by the particle size of the metal catalyst. Excessive metal catalyst particle size, such as greater than 8 nm, may also prevent CNTs synthesis [41].
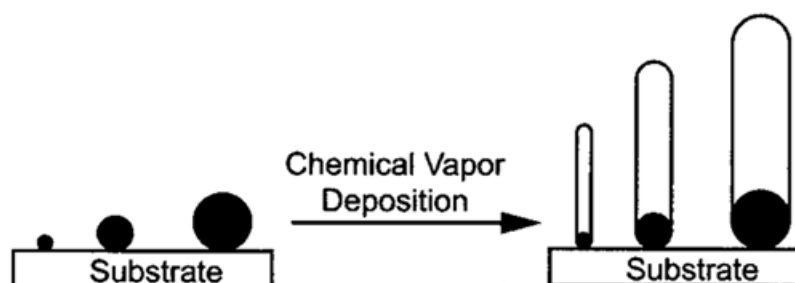
Figure 2. 6 The formation of CNTs depends on the size of the catalyst nanoparticles [42].

Initially, carbon source dissociative in carbon atom and other components, then carbon atom deposited on the catalyst surface until saturated condition. After that CNTs forming in two mechanism ; Tip growth and based growth. As shown in Figure 2.7, Tip Growth mechanism CNTs push the catalyst upward and form CNTs upward until the catalyst is encapsulated in the CNTs. Base growth type CNTs are formed with the catalyst attached on the support materials. The resulting CNTs form until there is no contact area between the reactants and the catalyst surface, in meaning of deactivation of catalyst by coke formation.
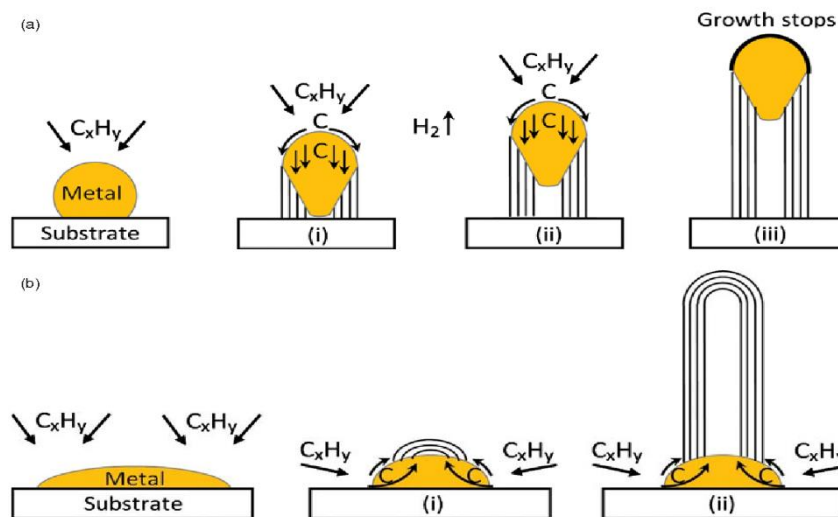
Figure 2. 7 The formaction mechanism of CNTs (a) Tip Growth (b) Base Growth [38]

2.5 H_2 production via catalytic decomposition of methane

The demand for hydrogen has been increasing in the last decades for use as clean energy. H_2 production has several route such as water splitting, steam reforming (SR), dry reforming (DR), water gas shift (WGS), CO_2 reforming, and catalytic decomposition of methane. Each method has its own disadvantages, such as consuming high energy (water splitting), resulting in green house gas (SR, DR, WGS). In other ways, the catalytic decomposition of methane, even consume a lot of energy

because operated at high temperatures (600-1000 °C) but this process is presented as a fully green one-step technology and valuable by-product carbon nanotubes. Therefore, researchers have developed a long-terms as possible CNTs production process to producing H_2 and getting higher yield of CNTs production [3, 4, 6, 43-47].
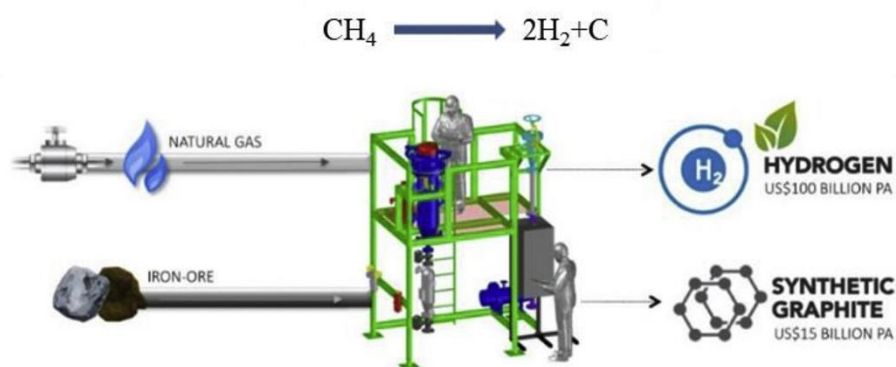
Figure 2. 8 H_2 production via catalytic decomposition of methane [47]

2.6 H_2 roles to synthesis of CNTs process

H_2 play a rather vague roles in the synthesis of CNTs. As shown in Table 2.1, summarized condition for the synthesis of CNTs from various researches, whether the fixed bed CCVD, FC-CVD (floating catalysts – chemical vapor deposition) or fluidized bed process with the aim to increasing productivity. Both of the production of SWCNTs and MWCNTs were included in Table 2.1.

Table 2. 1 Condition for the synthesis of CNTs

Catalyst	Feedstock	Product	Reduction of catalyst	references
$CoSO_4/SiO_2$	CO	SWCNTs	Yes	Wang, 2020 [48]
CoMo/quartz coating	$EtOH/H_2/Ar$	SW/DWCNTs	Yes	Inoue, 2018 [10]
$FeMo/SiO_2$	$C_2H_4/H_2/N_2$	MWCNTs	Yes	Chang, 2018 [9]

MetalSO$_4$/SiO$_2$ (Fe,Ni,Co)	CO/Ar	SWCNTs	No	Wang, 2018 [7]
Ferrocene+sulfur	CH$_4$/H$_2$/Ar	SWCNTs	No	Yadav, 2019 [49]
Fe/MgO	CH$_4$/He	SWCNTs	Yes	Abdullahi, 2014 [8]

It can be seen that in the CNTs synthesis process, there are either H$_2$ –free in the system [7], a process that uses H$_2$ for reduction of catalyst [8, 43, 48], and a process with both reduction of catalyst and co-feed H$_2$ during CNTs formation [9, 10]. Therefore, H$_2$ is expected to play a role in two ways: either directly affecting the formation of CNTs or affecting the catalyst, which further affects CNTs.

2.6.1 H$_2$ affected the CNTs formation

The study of H$_2$ roles or effect of H$_2$ to CNTs production has been studied for a long time. Firstly, the research of Piedigrosso et al. [11] reported H$_2$ caused hydrogenation that eliminated both of CNTs and amorphous carbon, from these report other research found that, the used of H$_2$ during CNTs synthesis increased yield of CNTs [12-18] because H$_2$ etched amorphous carbon out from catalyst surface that kept reaction still occur.

Piedigrosso et al.[11] shown the experiment of catalytic hydrogenation by used of as-prepared CNTs reacted with H$_2$/N$_2$ at 900°C. The resulted show in figure 2.9 and 2.10, that hydrogenation not only can eliminate part of the amorphous carbon but also destroys the CNTs too.
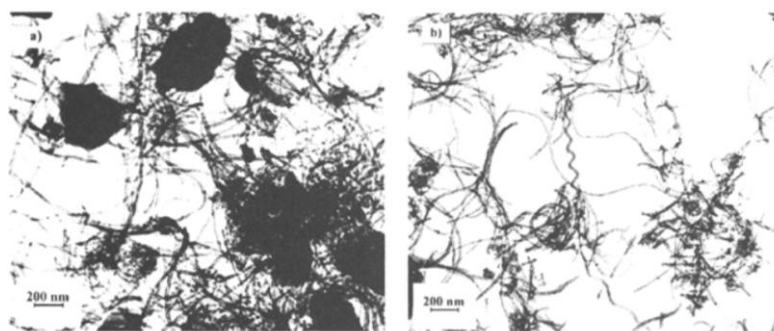
Figure 2. 9 Low magnification images of carbon nanotubes after hydrogenation in the conditions: H$_2$ flow 10 ml/min, N$_2$ flow 10 ml/min, temperature 900°C. a) amorphous

carbon is partially removed from the sample. B) Long and mainly short carbon
nanotubes [11]
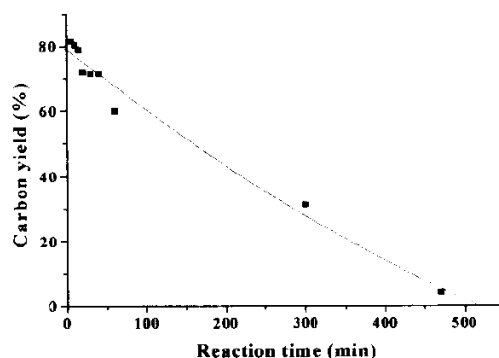
Figure 2. 10 Carbon yield variation versus reaction time in the following conditions :
H_2 flow 10 ml/min, N_2 flow 10 ml/min, temperature 900°C [11]

Topic of H_2 assisted to eliminate amorphous carbon often report with Raman
spectroscopy resulted by report an intensity ratio between graphitic carbon (I_G) and
disordered carbon (I_D), that should be increased when add H_2 into process, but some
researched found that adding H_2 decreased I_G/I_D ratio and hinder SWCNTs formation
[19]. Conducted the concentration of H_2 in feed gas is the important one, every
researched saw in the same way that concentration of H_2 has an optimal point. In
other words, too high H_2 concentration resulting in poor product both of yield and I_G/I_D
ratio, because H_2 is the one product from catalytic decomposition of carbon source
which include H_2 atom (methane, ethane, ethylene etc.), then the more H_2 feed the
more equilibrium shifted [14-16, 18, 50].

2.6.2 H_2 affected the catalyst

From the studied of Behr et al. [15], they studied the H_2-to-CH_4 ratio in feed
gas. They found in the same way as other research are adding a H_2 to process,
increasing length (yield of vertical align CNTs, VA-CNTs) and decreasing I_D/I_G ratio (same

as increasing of I_G/I_D) but they has further reported to the altered CNTs diameter size as shown in Fig 2.11 and 2.12.
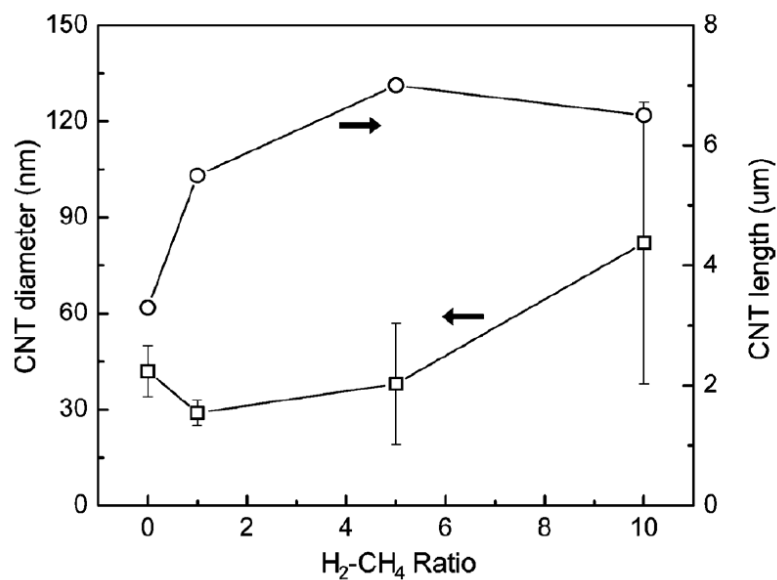
Figure 2. 11 Average CNT diameter, and CNT length as a function of H_2-to-CH_4 flow rate ratio. Error bars are the standard deviation for each sample and is a measure of the diameter distribution [15].
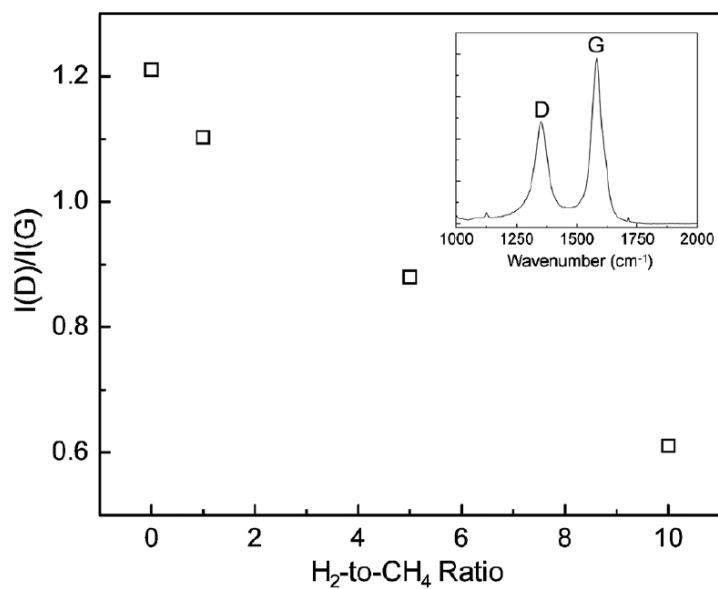
Figure 2. 12 Raman spectra (inset) from a MWCNT film. The ratio of the D and G peak intensities, I_D/I_G as a function of H_2-to-CH_4 flow rate ratio [15].

From the figure 2.11, CNTs diameter have increased in accordance with an increasing of H_2-to-CH_4 ratio. This is consistent with previous research in 2003 [19], 2007 [20] and 2008 [14, 20]. They reasoned that H_2-to-CH_4 ratio in the feed gas determines the relative fluxed of atomic H- and C-containing-species impinging on the catalysts, that resulting in determines the CNTs structure through the catalysts morphology and phase with the evidence as shown in Figure 2.13.
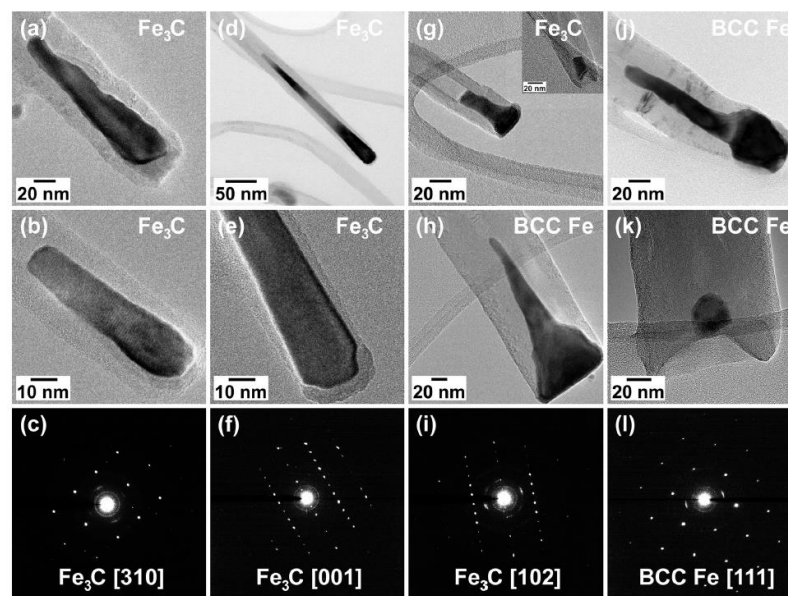
Figure 2. 13 BF-TEM images of (top two rows), and SAED patterns (bottom row) from, the most abundant catalyst crystals observed inside the base of MWCNTs grown using H_2-to-CH_4 flow rate ratios of (SCCM H_2: SCCM CH_4) (a)–(c) 0:5, (d)–(f) 5:5, (g)–(i) 25:5, and (j)–(l) 50:5 SCCM.

From Fig. 2.13, they used selected area electron diffraction (SAED) patterns and found that at low H_2-to-CH_4 ratio Fe-based catalyst trend to be Fe_3C and the increasing of H_2-to-CH_4 ratio made Fe-based catalyst to BCC Fe (α-Fe). This is why H_2 affects the catalysts that further affect to CNTs formation. Next to this research, He et al. [23] studied the catalyst morphology. They can determine Fe-based structure by controlling a reaction temperature in range 600-725 °C without reduction of catalyst, and found that lower reaction temperature (600-650 °C) trend to be Fe_3C and change

to at higher reaction temperature (650-725°C) **α**-Fe. After that they found that phase of catalyst severely affect to CNTs formation in terms of the yield, diameter and the most surprisingly, the appearance of the CNTs. They found that Fe_3C will made CNTs to bamboo like typed as shown in Fig 2.14 and 2.14
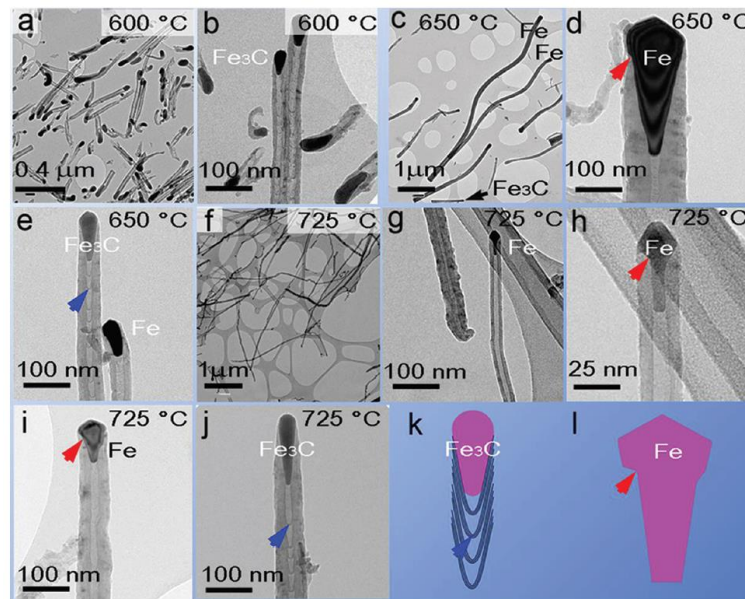
Figure 2. 14 Low-magnification and enlarged bright-field TEM images of CNFs/CNTs grown at different temperatures: (a, b) 600, (c–e) 650, and (f–j) 725 °C. (k, l) Schematics of Fe_3C and Fe catalyst shapes. Both Fe3C and Fe catalysts are elongated along the axis of the tubes/fibers, but the Fe_3C particles exhibit a rounded growth front which contrasts with the faceted one of the Fe particles. Note that both CNTs (h) and CNFs (j) have been observed at the high temperature growth of 725 °C [23].
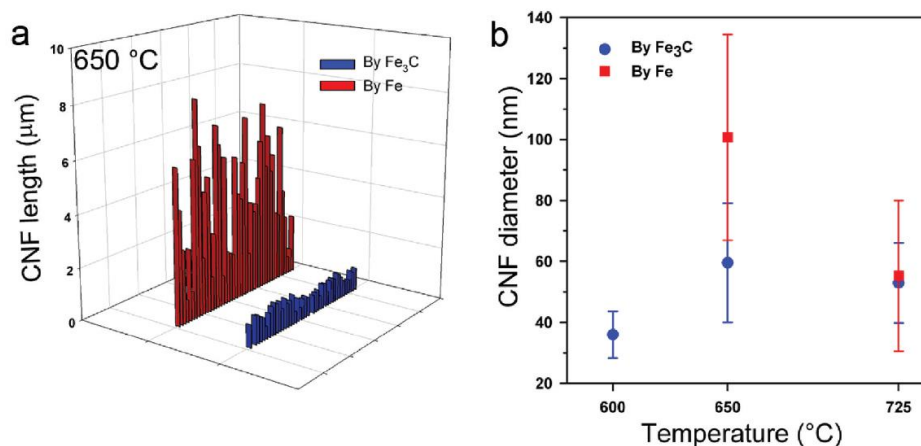
Figure 2. 15 Effect of Fe and Fe_3C on the growth of CNFs. (a) Plots of the measured lengths of CNFs catalyzed by Fe and Fe_3C at 650 °C. The length of CNFs was measured by TEM on randomly picked specimens. (b) Spreading of diameter values for CNFs/CNTs catalyzed by Fe and Fe_3C as a function of growth temperatures. Both the averaged values and standard error bars are shown [23].

After this research, Torres et al.[6] increased confidence in Fe_3C made CNTs to bamboo like by making a comparison between $Fe_{1-x}Co_x$ alloy with bcc crystal system and Fe_3C. They found that the process which making bamboo MWCNTs has lower yield as shown in Fig 2.16. However, adding of Co may be acted as active metal that increased yield in other ways.
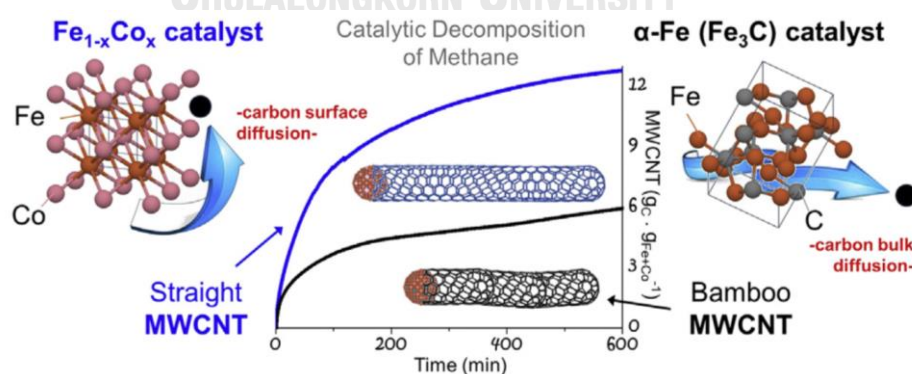
Figure 2. 16 Scheme of MWCNT formation by methane decomposition using a-Fe-based catalysts with (bottom) and without cobalt as a dopant [6]

From the reasonable evidence above, can explain previously researched why they found Bamboo CNTs [12] [24] or why H_2 added hinder [19] and decreased selectivity [20] of SWCNTs formation.

2.5 The kinetic study of CNTs synthesis

In general, the kinetic studies of CNTs are intended to study the mechanisms that determine the reaction and further use in scale-up to commercial scale. From the several research found that rate determining step of CNTs synthesis are mostly reaction rate controlled, that further differentiates which mechanism is limited the reaction. Each studied defines a different sequence of mechanisms such as Yadav et al. [33] defined as (1) Diffusion and mass transfer of carbon source (hydrocarbon gas, etc.) in the gas phase. (2) Catalytic decomposition of the hydrocarbon (surface reaction). (3) Surface or subsurface diffusion of carbon atoms over the active catalyst. (4) Supersaturation followed by precipitation of carbon molecules to form CNTs, or Robertson J. [51] defined as mass transport and reactions in the gas phase, dissociative absorption of the precursor molecule on the catalyst surface, diffusion of the resulting carbon atoms through the catalyst or over its surface, and finally precipitation of carbon atoms from the catalyst to form the growing nanotube as shown in Fig 2.17
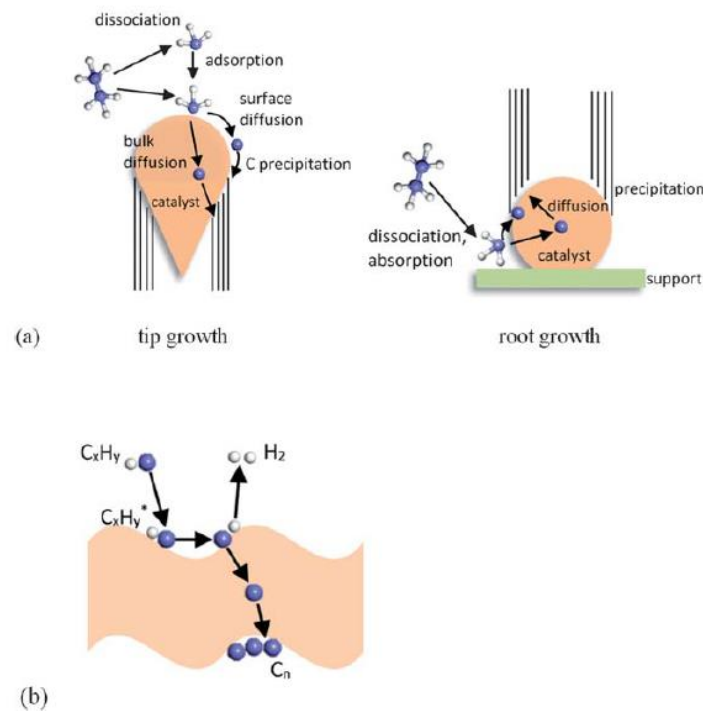
Figure 2. 17 (a) Processes in carbon nanotube growth, for tip growth and root growth and (b) Simplified model [51].

Yadav et al.[33] has investigated a several kinetic studied of CNTs that shown in Table 2.2. The kinetic study of CNTs favor report rate determining steps coupled with activation energies of their process. Synthesis of CNTs is the gas-solid-solid system, making it highly complex that is difficult to explain with a rate constant (k). In generally researchers used comparisons of activation energy to study the mechanisms of CNTs, such as comparing E_A from CNTs synthesis with E_A from reduction process of catalysts. In addition, it is difficult to collect data for use in kinetic study. This gives researchers a wide variety of ways to collect data. The simplest data collection method is the used of batch analysis by collect data on changing weight of the catalyst bed and using a reaction time to calculated for rate [52] [53]. The in-situ optical imaging is used to measure growth kinetics by real-time imaging but this method specified to VACNTs [54]. Another way to collect real time data is the gas phase analysis by collected

related gas such as the conversion of the reactants (CH_4) or the production of by-product (H_2) [55].

Table 2. 2 Rate determining steps and activation energies reported in literature for synthesis of carbon nanotubes [33].

Type of CNT	Carbon source	Catalyst	Type of reactor	Rate determining step	Temperature range (°C)	Activation energy (kJ/mol)	References
SWCNTs	CO	Ferrocene	FC-CVD without substrate	Bulk diffusion of carbon	804–915	134.11	Anisimov et al. (2010)
SWCNTs	C_2H_2	Fe/Al2O3	FC-CVD with substrate	Bulk diffusion of carbon	560–800	96	Wirth et al. (2009)
SWCNTs	C_2H_5OH	Co/Mo	FC-CVD with substrate	Bulk diffusion of carbon	750–825	144.72	Einarsson et al. (2008)
DWCNTs	CH_4	Fe-Mo/MgO	Fixed bed	Irreversible decomposition of adsorbed carbon	900–1000	58	Douven et al. (2011)
MWCNTs	C_2H_4	Fe-Co/Al$_2$O$_3$	Fixed bed	Elimination of hydrogen atom from adsorbed carbon	600–700	130	Pirard et al. (2007)
MWCNTs	C_2H_2	Fe/Al$_2$O$_3$ Ni/Al$_2$O$_3$	Fluidized bed	—	700–850	25.6 65.6	Hsieh et al. (2009a)
MWCNTs	CH_4	Co/MgO Co-Mo/MgO	Fixed bed	Dissociation of carbon source	500–800	96 156	Ni et al. (2006)
MWCNTs	C_2H_2	Fe	FC-CVD with substrate	Bulk diffusion of carbon	800–1100	125.52	Lee et al. (2002a)
MWCNTs	C_2H_2	Ni/CaCO$_3$ Co/CaCO$_3$	Fluidized bed	—	700–850	104.6 61.6	Hsieh et al. (2009b)
MWCNTs	C_2H_2	Fe/Carbon black	Fluidized bed	Formation of carbon molecules	700–807	47	Dasgupta et al. (2014)
				Diffusion through substrate pores	807–1000	7.6	
MWCNTs	CO_2	Fe/CaCO$_3$	Swirled FC-CVD	–		35	Simate et al. (2014)
MWCNTs	C_2H_4	Co-Fe-Mo/ Al2O3	Fluidized bed	–	650–730	102	Jeong et al. (2015)
MWCNTs	C_2H_2	Ferrocene	FC-CVD without substrate	Bulk diffusion of carbon	700–1000	146.4	Lee et al. (2003)
MWCNTs (N-doped)	FePc/CoPc/ NiPc	FePc/CoPc/NiPc	FC-CVD with substrate	Bulk diffusion of carbon	700–1000	125.5	Kim et al. (2003)
SWCNTs	CH_4	Ferrocene	FC-CVD without substrate	Surface reaction of carbon precursor on catalyst surface	800–1000	80.16	Present work

The system of CNTs synthesis in CVD need to used catalyst, the deactivation of catalysts is inevitable so to collect the real time kinetic data, researchers focused in the initial rate of reaction as shown the production of H_2 from the decompose of ethylene in Fig 2.18
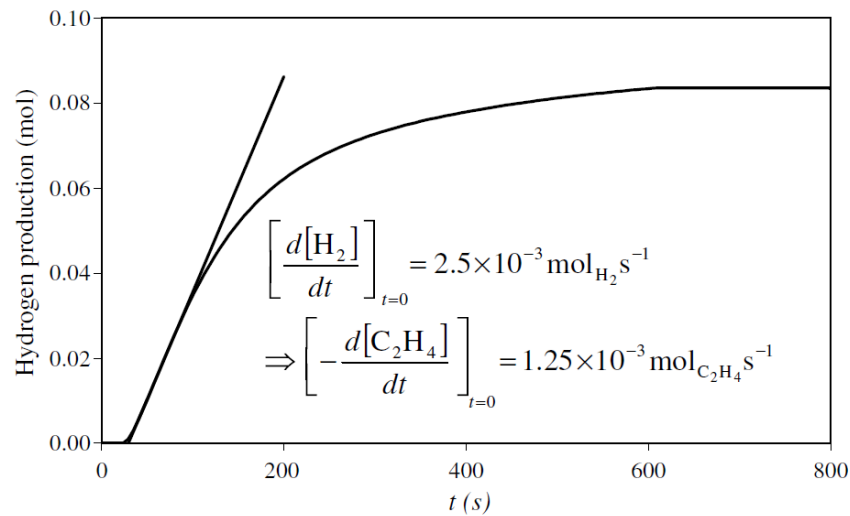
Figure 2. 18 Example of hydrogen production curve as a function of time and determination of initial reaction rate for a feed gas composed of x_{C2H4} = 30%, x_{H2} = 0%, and x_{He} = 70% [55].

Douven et al. [56] have a fairly comprehensive example of kinetic of cnt studies. They start with studying of mass transfer of process, firstly to investigated external mass transfer; the only operating variable that changes is the gas flow velocity, which directly impacts the mass transfer coefficient according to equation 2.1. Therefore, when adjusting the total flow, the effect of external mass transfer can be studied (Fig 2.19).

$$Sh = \frac{K_M l}{D_e} = CRe^{\frac{1}{2}} Sc^{\frac{1}{3}} \quad ; Re = ul/v \tag{2.1}$$
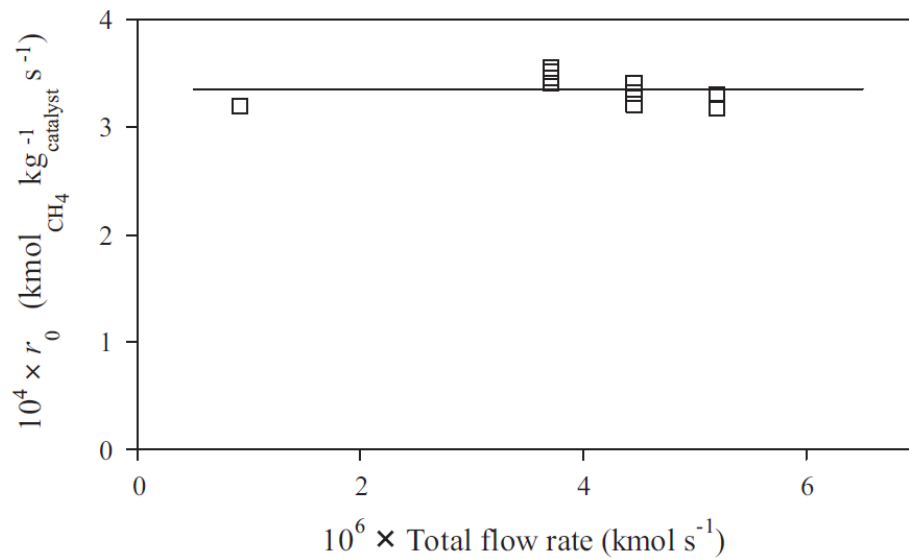
Figure 2. 19 Initial specific reaction rate, r_0, as a function of the total flow rate for P_{CH4} =0.6 atm, P_{H2}=0 atm, P_{He} = 0.4 atm at 900 °C [56].

From fig 2.19 shown that initial specific reaction rate, r_0 is not affected by the variation of the gas flow velocity in meaning that there are no external transport limitations. After that they studied internal mass transfer via the Weisz modulus φ compares the initial specific reaction rate. If $\varphi \ll 1$, methane diffusion is not the limiting factor and the operating regime is a chemical regime. If $\varphi \gg 1$, diffusion limitations occur in the catalytic bed and the operating regime is a diffusional regime. The Weisz modulus is defined by equation 2.2, the result shown in table 2.3

$$\varphi = \frac{r_0 \rho d_b^2}{D_e C_s} \tag{2.2}$$

Table 2. 3 Initial specific reaction rates r_0 and associated Weisz modulus φ with corresponding operating methane and helium partial pressures at 900 °C, 950 °C and 1000 °C [56].

	P_{CH_4} (atm)	P_{He} (atm)	$10^4 \times r_0$ (kmol$_{CH_4}$ kg$_{catalyst}^{-1}$ s^{-1})			Φ (−)		
			900 °C	950 °C	1000 °C	900 °C	950 °C	1000 °C
1	0.01	0.99	0.27	0.28	0.28	0.32	0.31	0.31
2	0.03	0.97	0.74	0.80	0.81	0.29	0.30	0.30
3–1	0.05	0.95	1.14	1.22	1.24	0.27	0.28	0.28
3–2	0.05	0.95	1.42	1.39	1.56	0.33	0.32	0.35
4–1	0.1	0.9	1.72	2.18	2.34	0.20	0.25	0.26
4–2	0.1	0.9	1.76			0.21		
5–1	0.2	0.8	2.52	3.12	3.39	0.15	0.18	0.19
5–2	0.2	0.8	2.39		3.18	0.14		0.18
6–1	0.3	0.7	3.26	3.63	4.15	0.13	0.14	0.15
6–2	0.3	0.7			4.23			0.16
7–1	0.4	0.6	3.49	4.10	4.82	0.10	0.12	0.13
7–2	0.4	0.6			4.82			0.13
8–1	0.5	0.5	3.30	4.26	5.18	0.08	0.10	0.11
8–2	0.5	0.5	3.30			0.08		
9–1	0.6	0.4	3.17	4.27	5.41	0.06	0.08	0.10
9–2	0.6	0.4	3.22			0.06		
10	0.7	0.3	3.16	4.01	5.55	0.05	0.07	0.09
11	0.8	0.2	3.09	3.98	5.07	0.05	0.06	0.07
12–1	0.9	0.1	2.78	3.76	4.94	0.04	0.05	0.06
12–2	0.9	0.1	2.82			0.04		
12–3	0.9	0.1	3.28			0.04		
12–4	0.9	0.1	3.06			0.04		
12–5	0.9	0.1	2.98			0.04		

From table 2.3, found that the highest φ is 0.35 which confirm that the absence of internal diffusion limitations determined experimentally.

Next, the kinetic study of CNTs will focused on sequences of elementary steps and choose a model to validate with experimental data. Yadav et al. [33] assuming dissociative adsorption of methane followed by removal of hydrogen from the adsorbed methyl group as the rate determining step with difference path ways, model 1 is one type of active site (x) and model 2 is two types (x and y). Models 1 and 2 lead to following rate equation 2.3 and 2.4. The reaction pathways for each model shown in Table 2.4. The kinetic model and their linear forms to find out rate constant (k) shown in Table 2.5, then the experimental and the simulated values from their model were plotted as shown in Fig 2.20.

Model 1　　　$R = \dfrac{k_1 P_{CH_4}}{\left[1 + \dfrac{k_1 P_{CH_4}}{k_2}\right]}$　　　　　　　(2.3)

Model 2　　　$R = \dfrac{k_1 P_{CH_4}}{\left[1 + \dfrac{k_1 P_{CH_4}}{k_2}\right]^2}$　　　　　　　(2.4)

Table 2. 4 Reaction steps in the dissociative adsorption pathways [33].

Model 1	Model 2
$CH_4 + x + y \xrightarrow{k_1} CH_3 - x + H - y$	$CH_4 + 2x \xrightarrow{k_1} CH_3 - x + H - x$
$CH_3 - x + y \xrightarrow{k_2} CH_2 - x + H - y$	$CH_3 - x + x \xrightarrow{k_2} CH_2 - x + H - x$
$CH_2 - x + y \xrightarrow{k_3} CH - x + H - y$	$CH_2 - x + x \xrightarrow{k_3} CH - x + H - x$
$CH - x + y \xrightarrow{k_4} C - x + H - y$	$CH - x + x \xrightarrow{k_4} C - x + H - x$
$C - x \xrightarrow{k_5} C + x$	$C - x \xrightarrow{k_5} C + x$
$2Hy \xrightarrow{k_6} H_2 + 2y$	$2Hx \xrightarrow{k_6} H_2 + 2x$

Table 2. 5 Kinetic models and their linear forms [33].

	Non-linear form	Linear form	Plot	Parameters
Model 1	$R = \dfrac{k_1 P_{CH_4}}{\left[1 + \frac{k_1 P_{CH_4}}{k_2}\right]}$	$\dfrac{P_{CH_4}}{R} = \dfrac{P_{CH_4}}{k_2} + \dfrac{1}{k_1}$	$\dfrac{P_{CH_4}}{R}$ vs. P_{CH_4}	k_1 = 1/intercept; k_2 = 1/slope
Model 2	$R = \dfrac{k_1 P_{CH_4}}{\left[1 + \frac{k_1 P_{CH_4}}{k_2}\right]^2}$	$\sqrt{\dfrac{P_{CH_4}}{R}} = \dfrac{P_{CH_4}\sqrt{k_1}}{k_2} + \dfrac{1}{\sqrt{k_1}}$	$\sqrt{\dfrac{P_{CH_4}}{R}}$ vs. P_{CH_4}	k_1 = 1/(intercept)^2; k_2 = 1/(slope x intercept)
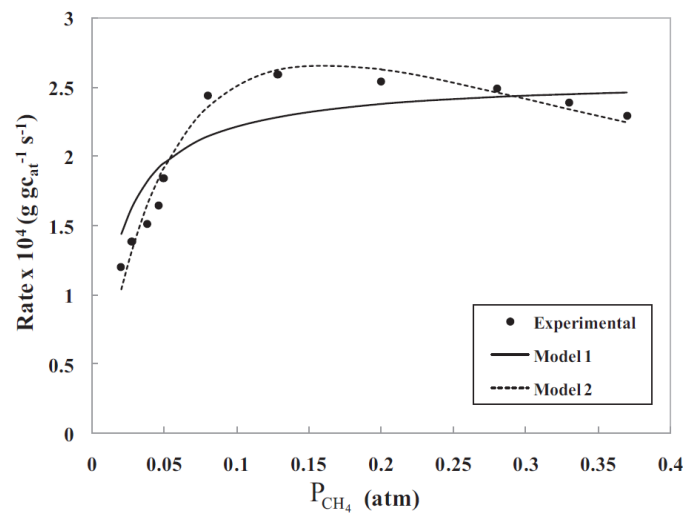
Figure 2. 20 Comparison of Model 1 and Model 2 for predicting the CNT formation rate at 1000 $^\circ$C [33].

After the apparent rate constant has been determined, use this information to find Activation energy (E_A) of assuming mechanism by changing the temperature followed equation 2.5 and 2.6

$$k_1 = k_{1ref} \exp\left[-\frac{E_{a1}}{R}\left(\frac{1}{T} - \frac{1}{T_{ref}}\right)\right] \tag{2.5}$$

$$k_2 = k_{2ref} \exp\left[-\frac{E_{a2}}{R}\left(\frac{1}{T} - \frac{1}{T_{ref}}\right)\right] \tag{2.6}$$

Douven et al. [56] defined E_{a1} and E_{a2} are the E_A of the first and the second elementary steps corresponding to model 2's dissociative adsorption pathways in table 2.4. They found that E_{a2} is the energy of irreversible decomposition of the adsorbed methyl group that equal to 58 kJ mol^{-1}, while the activation energy E_{a1} of irreversible dissociative adsorption of methane is not significantly different from zero (8±6 kJ mol^{-1}). From this result, the kinetic study of CNTs will be summarized which mechanism is the rate-determining step for this reaction. In other works, they summarized the limited mechanism more simply such as Ni et al. [52] reported the reaction order is unity, indicating that the dissociation of CH_4 on Co surface is the rate-determining step. There are other routes to find rate-determining step. For example, the activation energy of CNTs synthesis process is compared with other E_A processes such as E_A of CH_4 dissociative with varied catalyst, or E_A of reduction of catalyst or E_A etc. To verify the accuracy of the experimental results, they often compare the E_A values for each study, as shown in the table 2.2.

Chapter 3

Experimental

3.1 Catalyst preparation

FeMo/MgO catalyst with 30%wt metals loading prepared by impregnation method. The iron (III) nitrate nonahydrate ($Fe(NO_3)_3.9H_2O$, 98%, AR, Loba chem.) and ammonium heptamolybdate (($NH_4)_6Mo_7O_{24}$, AR, KEMAUS) solution were prepared as precursors of Fe and Mo with mass ratio of Fe:Mo equal to 2:1, then slowly drop of Mo solution into Fe solution to avoid precipitation. The FeMo solution was dropped on Magnesium oxide fine particle (MgO, pharma, Applichem Panreac.). The mixture was stirred and dried on hot plate stirrer at $90^{\circ}C$ until forming of paste, then dried in oven with the same temperature for 4 hours and calcination at $500^{\circ}C$ for 3 hours. The FeMo/MgO in oxide form is ready to use for the reaction. The images of the experimental process are shown in Figure 3.1.

I. Prepare Fe and Mo solution using 25 mL DI water per each.

II. slowly drop of Mo solution into Fe solution to avoid precipitation then will get clear

III. Dropped solution on MgO particle

III. Stir and dry on hot plate stirrer until become paste

IV. Dry in oven at $90^{\circ}C$ for 4 hours and crushed

V. Calcination at $500^{\circ}C$ for 5 hours
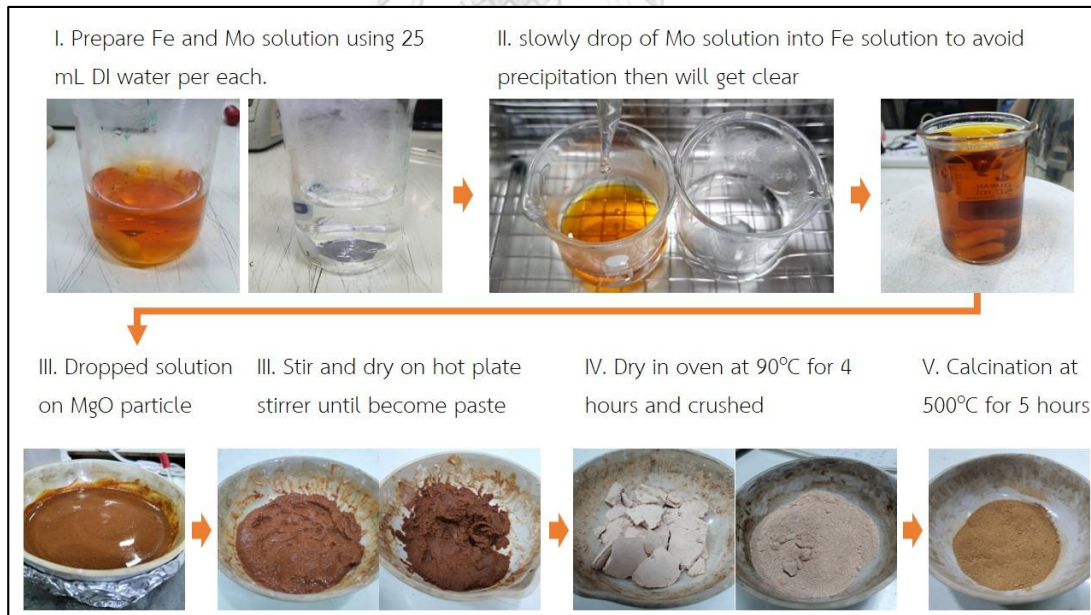
Figure 3. 1 Preparation of FeMo/MgO by impregnation method

3.2 Synthesis of CNTs

CNTs were synthesized by the catalytic chemical vapor-deposition (CCVD) method using methane as a carbon source. The schematic diagram was shown in Fig 3.2. Firstly, 0.5 g of FeMo/MgO catalyst was put in a quartz boat, then placed in the quartz tube reactor center. This CCVD process started with N_2 fed into the reactor and heated up at room temperature until it reached desired temperature by linearly increased at a rate of $10^{\circ}C/min$.
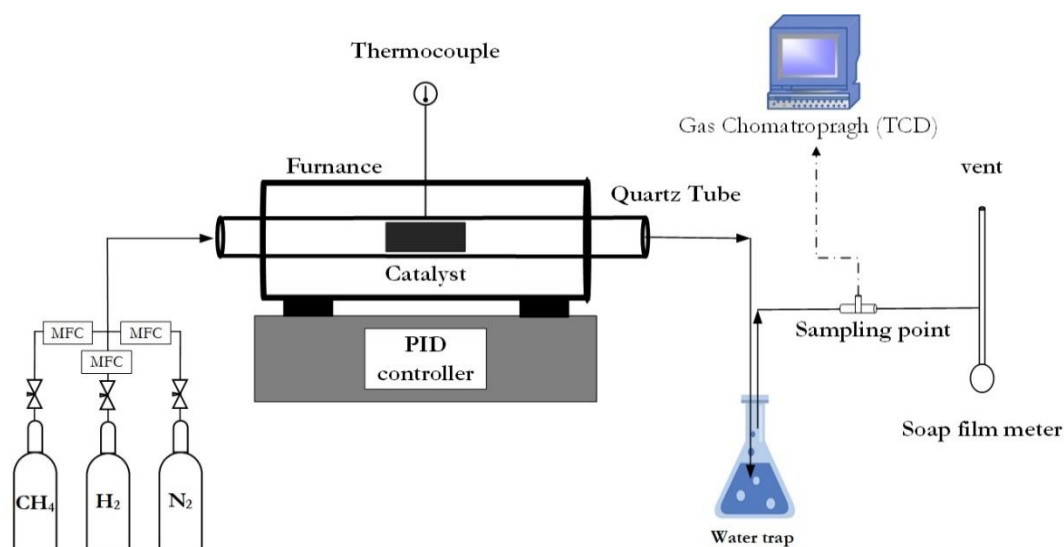
Figure 3. 2 Schematic diagram of CCVD method

The total gas flow rate was controlled following each process in Table 3.1, which calibrated by soap film meter. The effluent gas was collected and analyzed with Gas Chromatography (GC-TCD 8A, Shimadzu). Conditions for GC analysis were set as follows (3 mm $\varnothing$ ×2 m column, INJ/DET: 120°C, COL: 100°C, active carbon packing: 0.2 – 0.25 mm, and He carrier: 40 mL min^{-1}). Until the end of the reaction (60 minutes), the system was cooled to room temperature in N_2 gas flow. The CNTs were formed at the surface of the catalyst in the quartz boat.

The catalytic performance in terms of CH_4 conversion, Carbon yield and g-CNTs/g-catalysts were calculated according to Eqs. (3.1)-(3.3), respectively.

$$X_{CH_4}(\%) = \frac{[CH_4]_{in} \times F_{in} - [CH_4]_{out} \times F_{out}}{[CH_4]_{in} \times F_{in}} \times 100 \tag{3.1}$$

$$\text{Carbon yield }(\%) = \frac{\text{product weight (g)-catalyst weight (g)}}{\text{carbon feed (g)}} \tag{3.2}$$

$$\frac{\text{g-CNTs}}{\text{g-catalysts}} = \frac{\text{product (g)-catalyst weight (g)}}{\text{catalyst weight (g)}} \tag{3.3}$$

$$\text{Calculated } H_2 \text{ flow rate (ml/min)} = F_{outlet} - F_{N2} - F_{unreacted, CH4} \tag{3.4}$$

The kinetics investigation will used data from product yield to perform a rate of reaction, which calculated by Eqs. 3.5

r_{CNTs} = product weight (g) – (catalysts weight)

$$r_{CNTs}\left(gg_{cat.}^{-1} s^{-1}\right) = \frac{\text{product weight (g)-catalyst weight (g)}}{\text{catalyst weight (g)x reaction time (S)}} \tag{3.5}$$

Table 3. 1 Experimental setup

Process	Experimental	Reduction Phase 30-900 °C 40 min (150 mL/min)	Reaction Phase 900 °C 180 min (200 mL/min)
1. H_2 free process	nR-woH_2	N_2 = 150	CH_4:N_2 = 50:150
2. H_2 co-feed process	nR-wH_2	N_2 = 150	CH_4:N_2:H_2 = 50:50:100
3. H_2 pre-reduction process	R-woH_2	N_2:H_2 = 50:100	CH_4:N_2 = 50:150
4. H_2 combined process	R-wH_2	N_2:H_2 = 50:100	CH_4:N_2:H_2 = 50:50:100

3.3 Characterization method

3.3.1 Study of morphology, internal and external structure

The study of morphology, internal, and external structure were examined using imaging process. The external structure of as-prepared and purified product were observed by Field Emission Scanning Electron Microscopes (FE-SEM, HITACHI SU-8010)

and Atomic force microscope (AFM). The internal structure, type of CNTs, number of walled, CNTs growth mechanism (Tip, based growth), CNTs and catalyst diameter size were observed by Transmission electron microscopes (TEM, JEOL JEM-2100 Plus). Sample preparation for TEM analyzed was prepare by following step; The product was dispersed in ethanol (99.5v/v%, Sigma-Aldrich) and then dropped onto a 300 mesh of copper grid coated with carbon film. As-prepared CNTs and catalysts diameter size were measured from SEM, AFM, and TEM images by using ImageJ software.

3.3.2 Crystallinity and structure analysis

Crystallinity and structure of CNTs and catalysts were analyzed for study changing in the sample, as a result of the controlled processes. X-ray diffraction (XRD) with the angle range scan 5°- 80° and TEM selected area electron diffraction (SAED) were used to specify crystallinity, phase change, crystal size included with crystallinity of the synthesized carbon products, which validated with qualitative analysis of the proportion between crystalline carbon and amorphous carbon was carried out using 532 nm laser light source Raman spectroscopy (Raman NT-MDT model: NTEGR-SPECTRA).

3.3.3 Reducibility and phase change mechanism of catalyst

The reduction mechanism of the catalyst was analyzed by H_2-TPR and XPS to study the reducibility of catalyst. This supporting to the suitable condition for reducing of catalyst to be desirable phase of catalyst by varying temperature and reaction time of the reduction process.

3.3.4 Purity and composition analysis

The purity of as-prepared product was measured from the thermo-gravimetric analysis (TGA), by observed the weight loss in expected temperature range. The composition of CNTs and catalyst were measured by EDS from SEM and TEM images.

Chapter 4

Results and discussion

In this work, synthesis of CNTs was examined by catalytic chemical decomposition (CCVD) of methane over FeMo/MgO catalyst. The study will be divided into two parts: studying the role of hydrogen and a kinetic study of the CNTs synthesis.

4.1 Roles of hydrogen

From the various researches, mentioned in the chapter 2, the roles of H_2 are often discussed in two areas which are, direct effect on the formation of CNTs to improve process yield and increase the crystallinity ratio of CNTs product, and effect to the catalyst that related to the characteristics of CNTs. Therefore, the design of the experimental process to study roles of H_2 to cover various hypotheses, the study was divided into 3 parts as follows: Effect of H_2 process, effect of H_2 concentration and hydrogenation reaction.

4.1.1 Effect of H_2

In the study roles of H_2, there are two variables that need to be studied which are, the pre-reduction of catalyst and the H_2 feeding during CNTs formation. Four processes: H_2 free process (no pre-reduction process and without H_2 feed during CNTs formation, nR-woH$_2$), H_2 co-feed process (no pre-reduced process and with H_2 feed during CNTs formation, nR-wH$_2$), H_2 pre-reduction process (pre-reduction process and without H_2 feed during CNTs formation, R-woH$_2$), and H_2 combined process (pre-reduction process with H_2 feed during CNTs formation, R-wH$_2$) with more details in Table 3.1, were used to investigated H_2 roles through catalytic activity and product properties with following results.

4.1.1.1 Conversion and yield

The catalytic activity was examined over CCVD for synthesis of CNTs process. From the experiment, FeMo/MgO catalyst is capable of converting CH_4 in all processes as shown by methane conversion in Fig. 4.1.
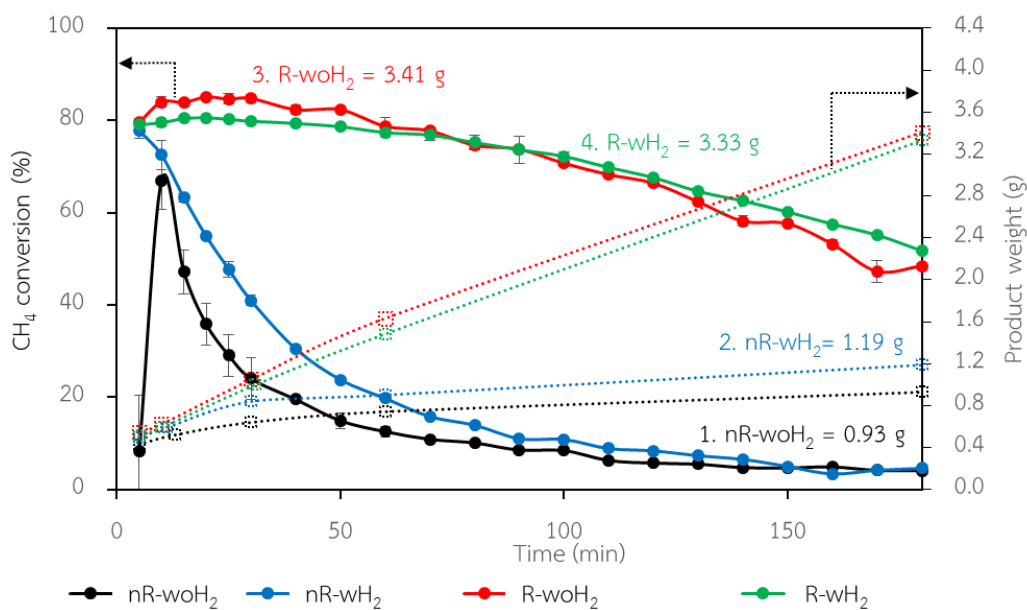
Figure 4. 1 Catalytic activity through (solid line) Methane conversion and (dotted line) product weight

Methane conversions decreased over time because of catalyst deactivation. The formation of product CNTs obstructed the active surface of catalysts. The catalyst performance depends on methane conversion, deactivated rate and quantity of final product. It was found that R-woH$_2$ was the most effective process with a 3.41 g final product followed with R-wH$_2$ (3.33 g), nR-wH$_2$ (1.19 g), and nR-woH$_2$ (0.93 g) respectively. The thermal stability of product was observed with thermo-gravimetric analysis (TGA) in air atmospheric, as shown in Fig. 4.2.
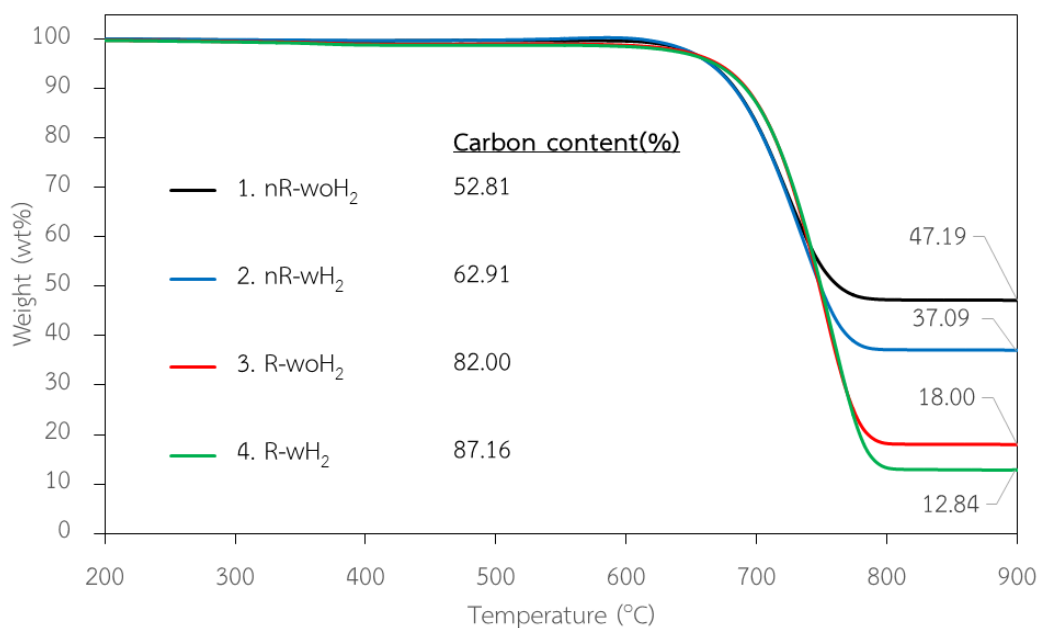
Figure 4. 2 TGA of as-prepared CNTs by comparing each H_2 processes.

From fig. 4.2 found that, product begins to decompose at temperatures of 600 $^\circ$C and above. Decomposition curves showed similar decomposed characteristics or referring to the same group of products. Residual from decomposition under air atmospheric are catalyst and supported materials which are highly thermal stability than carbon product, therefore we can get carbon content from TGA. The percentage carbon content corresponds to the yield. Product from pre-reduction of catalyst process (R-woH$_2$, R-wH$_2$) have higher carbon content than non-reduced process.

4.1.1.2 Morphology

The morphology of as-prepared products from various processes was investigated by image processing through scanning electron microscope (SEM) as shown in fig 4.3.
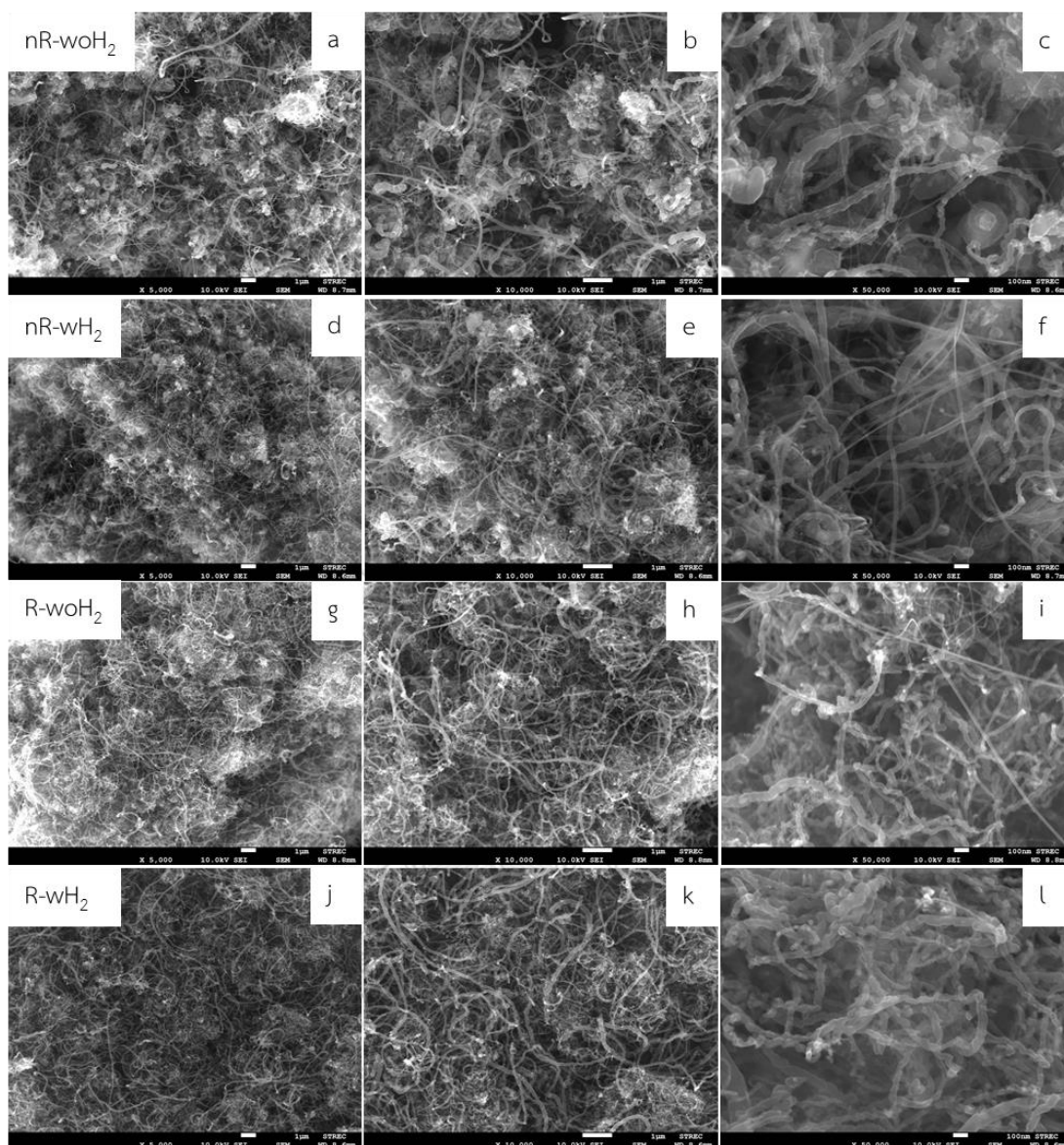
Figure 4. 3 SEM images of as-prepared CNTs from (a-c) nR-woH$_2$, (d-f) nR-wH$_2$, (g-i) R-woH$_2$, (j-l) R-wH$_2$ with magnification (a, d, g, j) 5,000x., (b, e, h, k) 10,000x., and (c, f, i, l) 50,000x.

Dense CNTs were found in all SEM images included with some amorphous carbon. Consider the CNTs product, the diameter of MWCNTs was measured from over 200 samples at 10,000x. magnification combined with over 100 samples at 50,000x. magnification by using ImageJ software to produce a diameter size distribution of as-prepared CNTs from each processes as shown in fig 4.4.
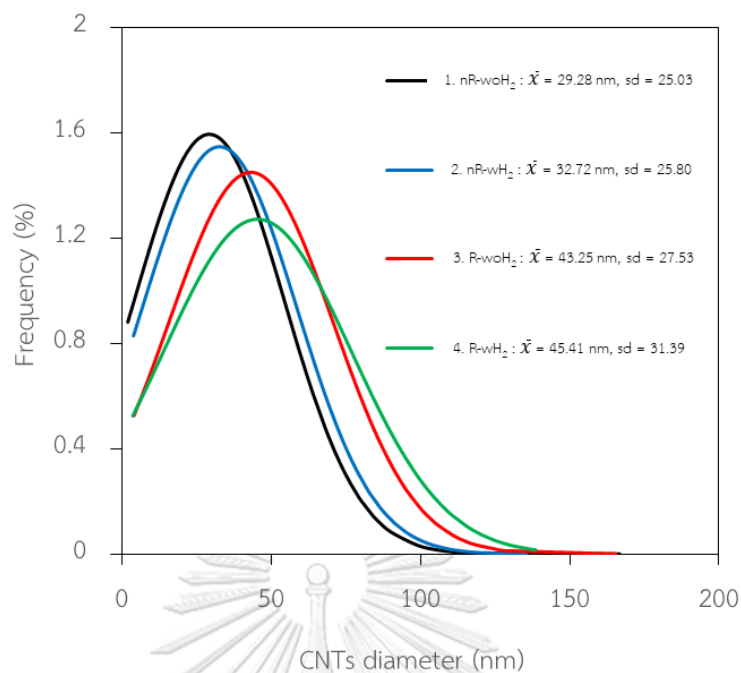
Figure 4. 4 CNTs diameter size distribution measured from SEM images.

The diameter size distribution of CNTs represents non-uniform product, ranging from tiny CNTs (smaller than 5 nm) to huge CNTs (larger than 100 nm), as a result of improper catalyst preparation method, thus affecting the active size which is expressed as the diameter of CNTs [42]. Considering the mean diameter, CNTs from non-reduced processes: nR-woH$_2$ and nR-wH$_2$ were approximately the same sizes (29.29 and 32.72 nm) meanwhile, the reduced process: R-woH$_2$ and R-wH$_2$ have similar in diameter (43.25 and 45.41 nm) but were larger than CNTs-nR processes.

4.1.1.3 Crystallinity

Qualitative analysis of the proportion between crystalline carbon and amorphous carbon was carried out using 532 nm laser light source Raman spectroscopy. Raman is used to determine proportions between graphitize carbon and disorder or amorphous carbon by the relative height of G band ($\sim$1580 cm^{-1}) and D band ($\sim$1350 cm^{-1}) that represent graphitic and disorder carbon, respectively. The G/D peak intensity ratios (I$_G$/I$_D$) of a carbonaceous product were investigated more than 5

points for each process to confirm the results of the analysis and prevent false sampling. Examples of the Raman analysis result are shown in Figure 4.5.
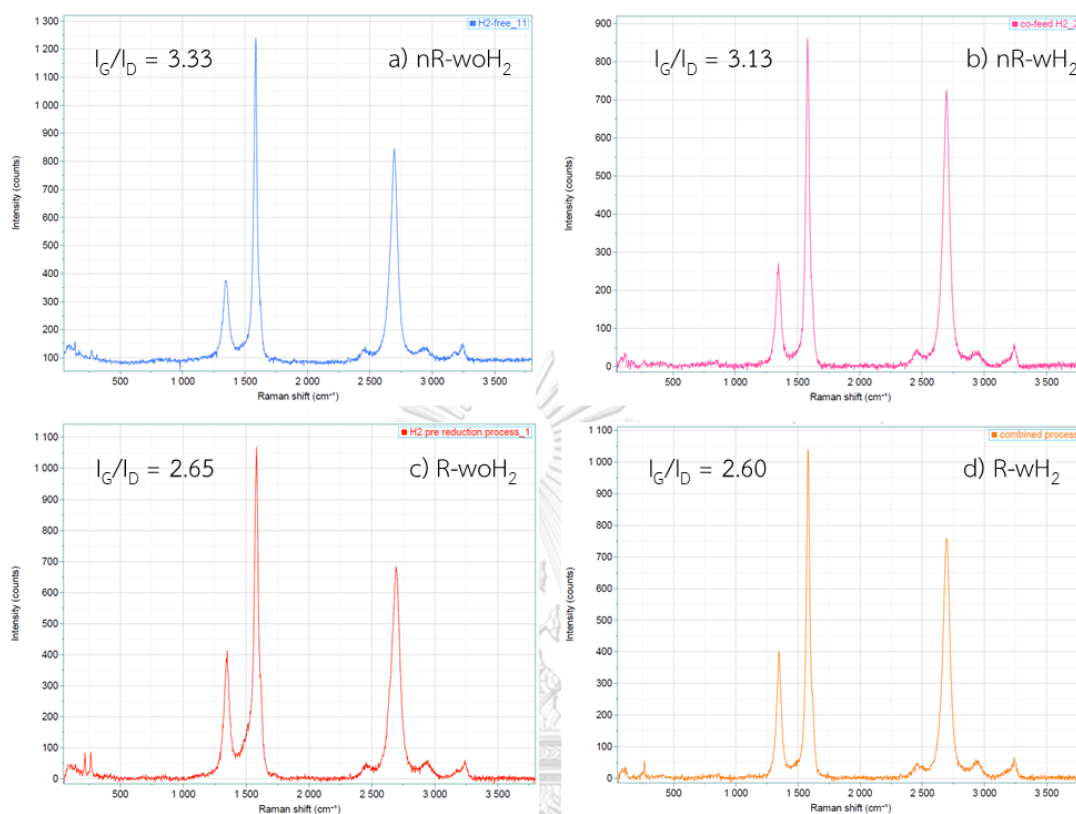
Figure 4. 5 Examples Raman characteristic of as-prepared CNTs

Average I_G/I_D ratio and other detailed data for the study of overview H_2 roles are shown in Table 4.1

Table 4. 1 Summary data for the study of overview H_2 roles.

Experimental	%yield	g-CNTs/g-catalysts	%C content (TGA)	Average diameter size (nm)	Avg. I_G/I_D
1. nR-woH$_2$ (H$_2$-free process)	10.16	0.85	52.81	29.28 ± 25.03	3.14 ± 0.61
2. nR-wH$_2$ (H$_2$ co-feed process)	15.85	1.37	62.91	32.72 ± 25.80	3.07 ± 0.49
3. R-woH$_2$ (H$_2$ pre-reduction process)	67.77	5.77	82.00	43.25 ± 27.53	2.58 ± 0.49
4. R-wH$_2$ (H$_2$ combined process)	64.88	5.61	87.16	45.41 ± 31.39	2.56 ± 0.24

From the Raman analysis, it was found that the products formed by non-reduced processes have higher I_G/I_D ratio than reduced processes which approximately are 3.1 and 2.5, respectively. Observed that the addition of H_2 during the formation of CNTs did not cause a difference in the crystallinity ratio (more detailed in section 4.1.3). Therefore, there was a possibility that the crystallinity ratio was also controlled by the catalyst structure.

It can be seen that, in the study of H_2 roles, the samples were clearly divided into two groups which are non-reduced processes and reduced process. Non-reduced process (nR-woH$_2$ and nR-wH$_2$) produces products with smaller diameters and higher crystallinity ratios than reduced processes (R-woH$_2$ and R-wH$_2$), but reduced processes have a higher yield than 5 times (~1 to ~5) of non-reduced process.

4.1.1.4 Structure of catalyst

The structure of the catalyst and as-prepared product in each process were investigated by XRD method to describe the mechanisms that cause changes in CNTs. Firstly, the H_2-temperature programmed reduction (H_2-TPR) analysis was used to investigate H_2 consumption during temperature changes, which is a similar experimental to pre-reduction of catalyst process. In the reduced process, it was confirmed by H_2-TPR that pre-reduction of catalyst from room temperature to 900 ^{o}C would allow the catalyst to remain structurally stable or without structural changes in the presence of hydrogen in the system [3], as shown in Fig2. 5, that H_2 is not consumed at 900°C and above.

XRD patterns of catalysts consisted of calcined MgO, calcined FeMo/MgO, and reduced FeMo/MgO are shown in Fig 4.6. The catalyst phases were identified by the diffraction peaks. The diffraction peaks of magnesium oxide (MgO, PDF 01-071-1176) were observed in Fig. 4.6a which were cubic structures. Fig 4.6b exhibited the diffraction peaks of MgO impregnated with iron (Fe) and molybdenum (Mo), where only monoclinic MgMo$_4$ at 23.2^o (021), and 26.3^o (220) [57] was found. Xu et al. [39] reported

an XRD analysis of calcined FeMo/MgO in Fig. 2.4, revealing the structure of MgO, Fe_3O_4, and $MgMo_4$. The results of the xrd diffraction were similarly blunt same as this work. XRD patterns of reduced FeMo/MgO was show in Fig 4.6c, tetragonal FeMo exhibited the diffraction peak at 37.3^o (002), 44.6^o (411), and 64.7^o (223) [58].
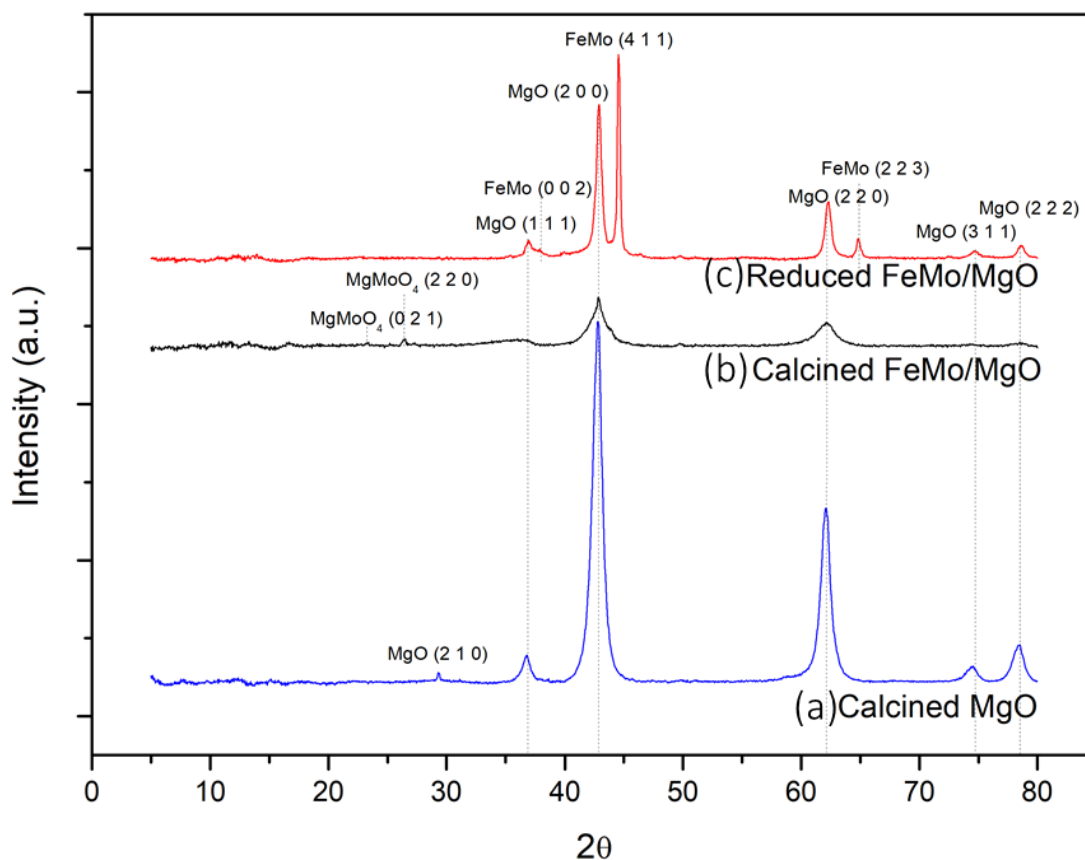
Figure 4. 6 XRD patterns of a) calcined MgO b) calicned FeMo/MgO
c) reduced FeMo/MgO

Fig 4.6 found that the calcination process did not detect Fe-Mo interaction, FeMo was found after the catalytic reduction process. Therefore, the reduction of catalyst process changes the catalyst structure from the oxide form to metallic structure and establishes an interaction between iron and molybdenum.

4.1.1.5 Structure of as-prepared product

Comparison of product structure between reduced FeMo/MgO, non-reduced CNTs (nR-woH$_2$), and reduced CNTs (R-woH$_2$) is shown in Fig. 4.7. FeMo undetectable after CNTs growth from both of non-reduced and reduced processes, which may cause by carbon obscuring or active metal was encapsulated within CNTs. Diffraction patterns of hexagonal carbon or carbon nanotubes was found at 25.9° (002) [59], which shown in Fig. 4.7b and 4.7c.
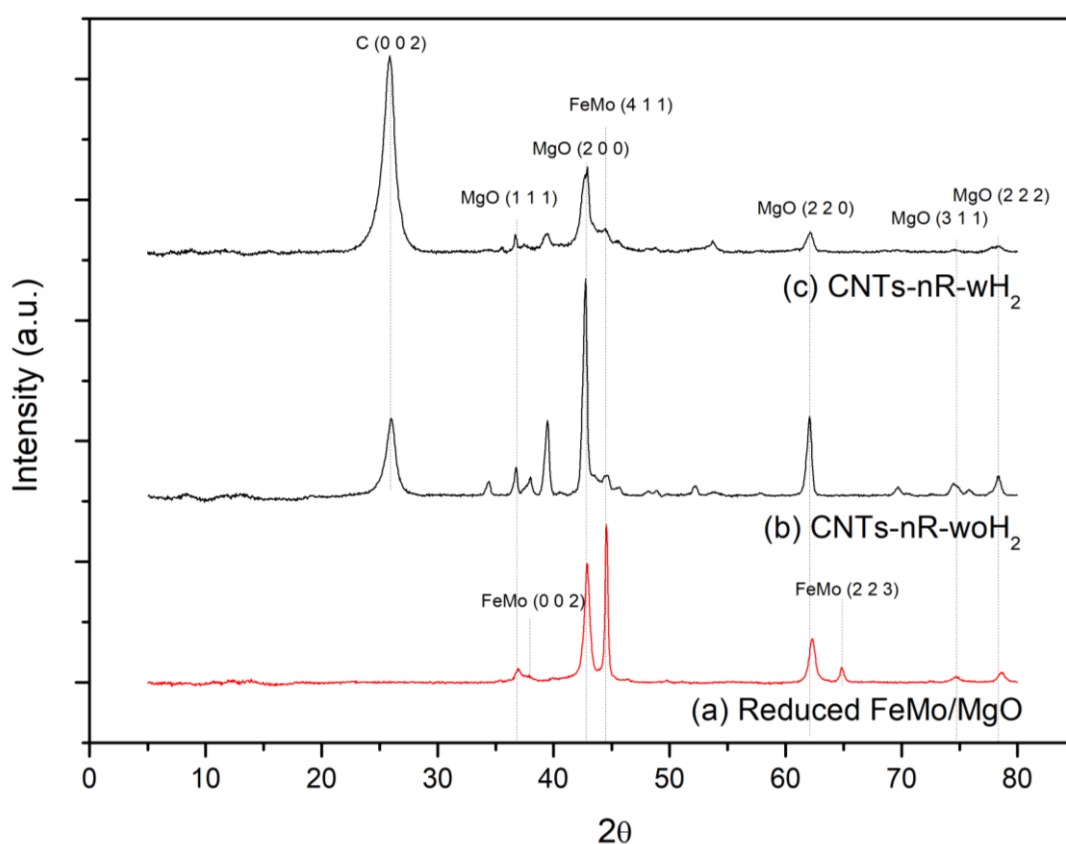
Figure 4. 7 Comparing XRD patterns of a) reduced FeMo/MgO b) CNTs-nR-woH$_2$
c) CNTs-nR-wH$_2$

XRD patterns of as-prepared CNTs for the study of H$_2$ roles are shown in Fig 4.8. It can be seen that the product characteristics are divided into two groups in the same

way as the properties of CNTs, which are non-reduced processes and reduced processes.
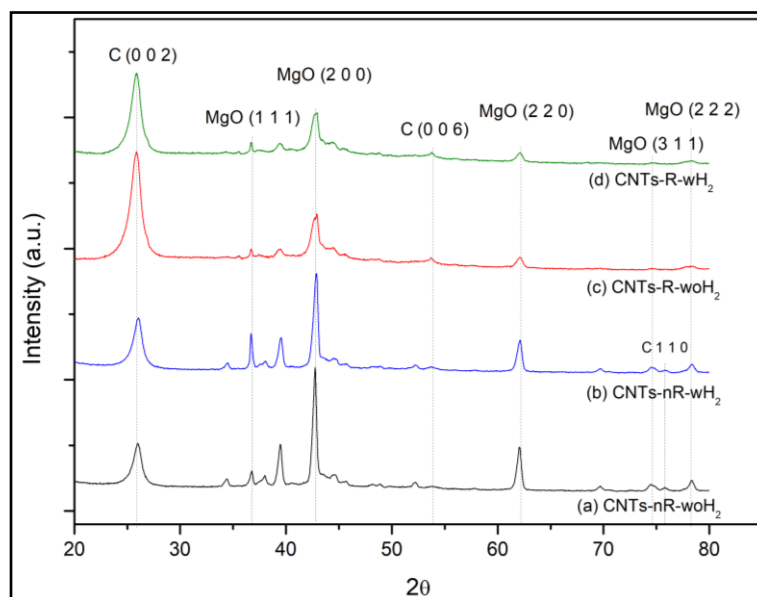
Figure 4. 8 XRD patterns of as-prepared CNTs from a) nR-woH$_2$, b)nR-wH$_2$, c) R-woH$_2$, d) R-wH$_2$

The details of the XRD analysis results in the 30°-60° and 68°-80° ranges are shown in Fig. 4.9A and 4.9B, respectively. The diffraction pattern exhibited iron carbide (Fe$_3$C) that can be found in all processes. Meanwhile, diffraction peak of molybdenum carbide (Mo$_2$C) are discovered in non-reduced processes. Therefore, in a non-reduced process, the catalyst is converted from oxide to carbide form. In addition, iron and molybdenum poorly interacted, resulting in the formation of molybdenum carbide structures. These results show why synthesized CNTs by non-reduced and reduced processes differ.
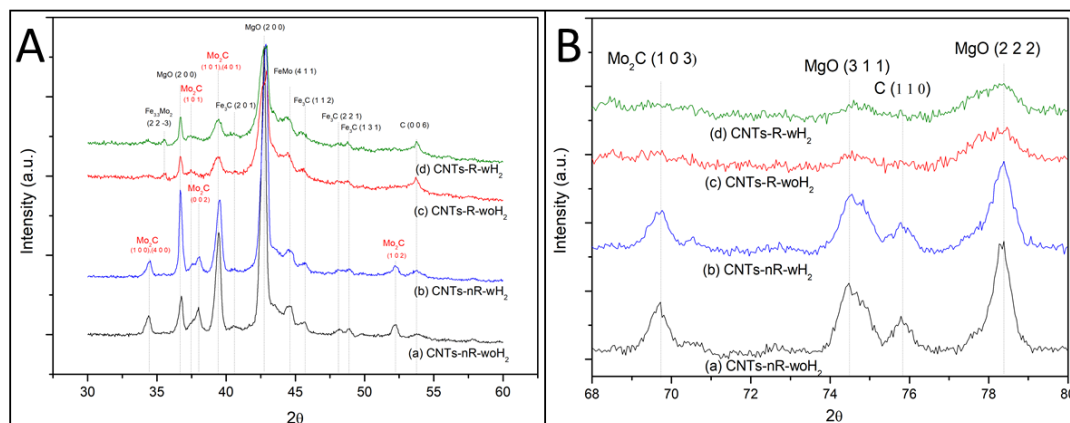
Figure 4. 9 XRD patterns of as-prepared CNTs in ranges (A) 30°-60° (B) 68°-80° from a) nR-woH$_2$, b)nR-wH$_2$, c) R-woH$_2$, d) R-wH$_2$

Several previous studies have mentioned similar behaviors with Fe catalysts. He et al. [23] reported that the carbide catalyst (Fe$_3$C) will make CNTs with a smaller diameter but lower yield than the metallic catalyst (α-Fe). In this work, we found that non-reduced processes will be made the carbide catalyst but reduced processes will be made metallic catalyst (FeMo). This is why products from the non-reduced and reduced processes are different.

The carbide formation of catalyst is described by Behr et al. [15], they studied the H$_2$-to-CH$_4$ ratio in the feed gas. Carbide formation will occur when lower H$_2$ –to – CH$_4$ ratio, while the metallic formation will occurred when a higher H$_2$-to-CH$_4$ ratio. Reduced processes in this work occur in H$_2$ and N$_2$ atmosphere, in the meaning there is no carbon (CH$_4$) in the system, that made a FeMo metallic, but for non-reduced processes, catalyst will be reduced by H$_2$ gas dissociated from CH$_4$, because CH$_4$ can be decomposed by the oxide form of the catalyst [60]. The reaction product hydrogen gas may make the reduction form of the catalyst with presence of carbon atoms in an atmosphere that caused a carbide catalyst.

Therefore, from the study of H_2 roles, it was found that the characteristics of CNTs, whether yield, diameter, and proportion of crystallinity, are determined by the structure of catalyst that was controlled by the pre-reduction process.

4.1.2 Effects of H_2 concentration

Effects of H_2 concentration were studied with H_2 co-feed or nR-wH$_2$ process. The catalytic performance was investigated at varied CH_4:H_2 ratio which are 1:0 (50:0 ml/min, nR-woH$_2$), 2:1 (50:25 ml/min), 1:1 (50:50 ml/min), 1:2 (50:100 ml/min, nR-wH$_2$), and 1:3 (50:150 ml/min). N_2 was used to adjust total flow rate to 200 ml/min. Methane conversion was investigated and shown in Fig. 4.10. H_2 flow rate was calculated by equation 3.4 and plotted against reaction time as shown in Fig. 4.11. As-prepared CNTs were measured for average diameter and summarizing the results with other information in Fig 4.12 and Table 4.2.
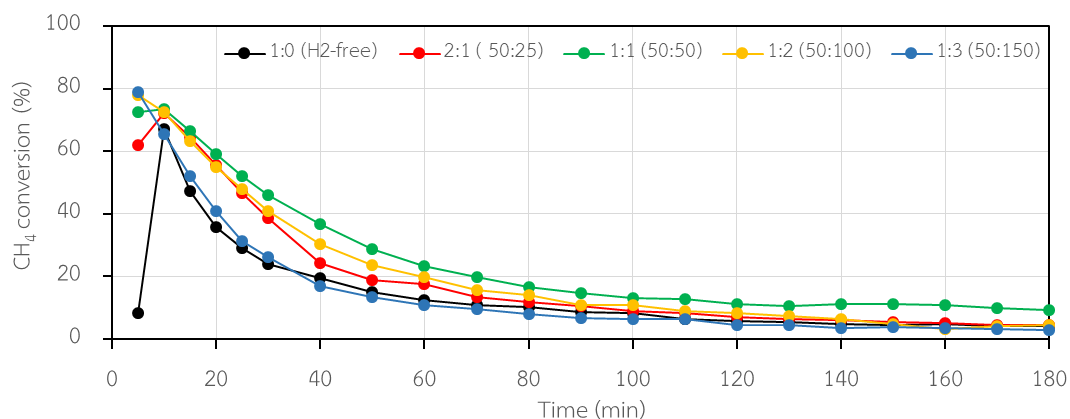
Figure 4. 10 CH_4 conversion over 30%loading FeMo/MgO at 900°C varied H_2 concentration
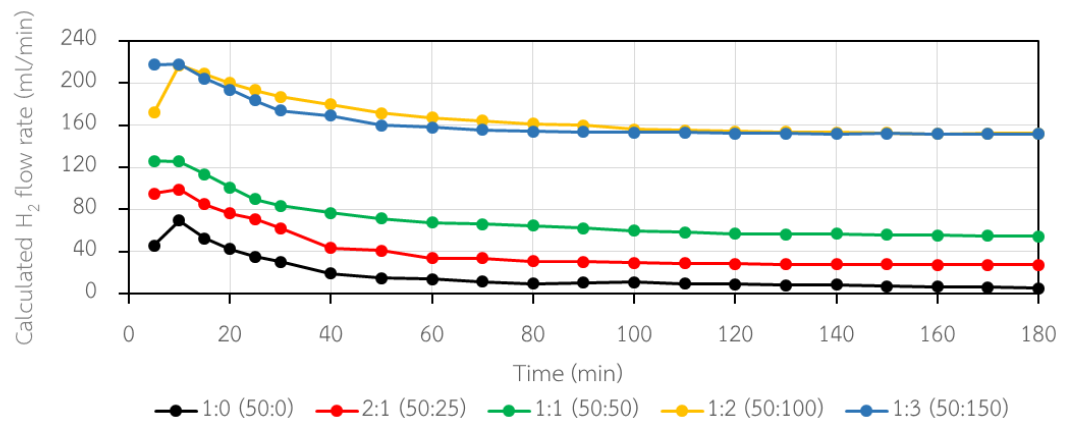
Figure 4. 11 Calculated H_2 flow rate over CNTs synthesis varied H_2 concentration
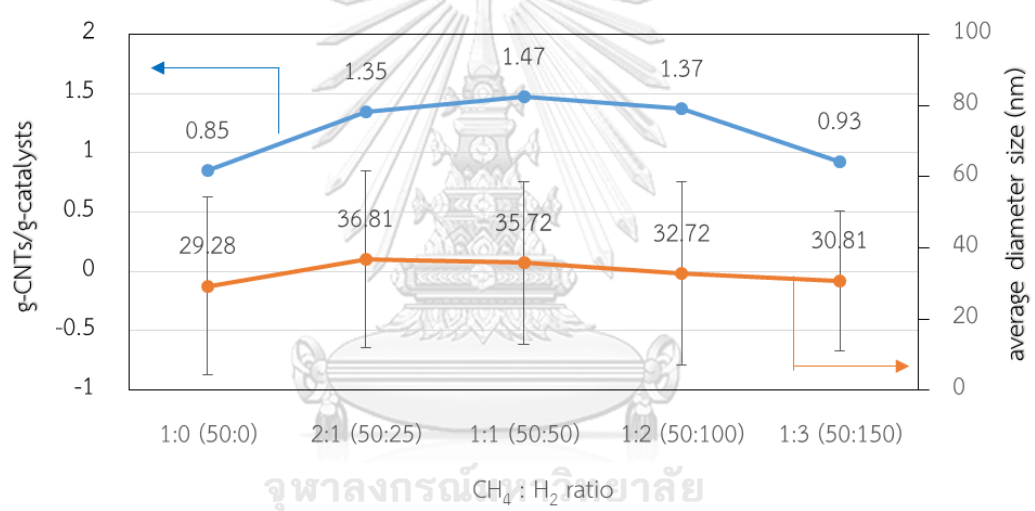
Figure 4. 12 g-CNTs/g-catalyst, and average CNT diameter as a function of CH_4:H_2 flow rate ratio. Error bars are the standard deviation for each sample and is a measure of the diameter distribution

Table 4. 2 summary data for study of effects of H_2 concentration

$CH_4 : H_2$	product weight	%yield	g-CNTs/ g-catalyst	average diameter size (nm)	sd. (nm)
1:0 (50:0)	0.9294	10.16	0.85	29.28	25.03
2:1 (50:25)	1.1763	17.06	1.35	36.81	24.72
1:1 (50:50)	1.2401	17.06	1.47	35.72	22.82
1:2 (50:100)	1.1889	15.85	1.37	32.72	25.80
1:3 (50:150)	0.9669	10.51	0.93	30.81	19.64

Methane conversion in each H_2 concentration was slightly different as shown in Figure 4.10, where the CH_4:H_2 ratio was 1:1 with the highest methane conversion. In Fig 4.11, exhibited H_2 flow rate that is higher than amount of H_2 feed into the system. Since H_2 is one of the products resulting from the decomposition of methane, it can be seen that H_2 flow rate decreases over time corresponding to the reduced methane conversion.

Fig. 4.12 shows the yield of the produce (g-CNTs/g-catalyst) with an optimum point of 1:1, corresponding to the conversion of methane. When the H_2 content is increased above 1:1, the yield is less. Observing at the flow rate of H_2, found that there are high amount of H_2 in system. The study of Kashiwaya Y., and Watanabe M. reported that methane decomposition is reversible reaction in gas phase before CNTs growth [61]. Therefore, according to Le Chatelier's principle, when the product quantity (H_2) increases, will prevent the dissociation of methane, resulting in fewer CNTs [46],[62]. Additionally, the addition of the proper amount of H_2 allows catalyst to restructure that ready for the formation of higher CNTs. Observed from H_2-free process (nR-woH$_2$) with the lowest methane conversion (∼8%) at 5 min, then the conversion increased. Because initially the catalyst was in an oxide form with lower methane conversion

performance, and when partially H_2 was formed, the catalyst changed its structure and thus the conversion increased.

The results of the study on adjustment concentration of H_2 gas, when adding H_2, yield was higher but decreased when excess H_2. Therefore adding H_2 to CNTs product has an optimal point, that consistent with various research [12-18].

Measure and establish the CNTs diameter size distribution from the study of effects of H_2 concentration as shown in Fig 4.11 and Table 4.2, found that as-prepared CNTs from this work are highly distributed. As a result, it was unable to confirm the results of the study of the diameter changes from the adjustment of the H_2 concentration.

However, a number of studies indicate that H_2 addition helps to eliminate amorphous carbon as well as maintain catalyst stability. To study about this issue, the study of catalytic hydrogenation reaction was conducted in the next section.

4.1.3 Hydrogenation reaction

This section examined the catalytic hydrogenation reaction that was thought to play an important role in the synthesis of CNTs, by investigating whether this reaction can help stabilize the catalyst during the synthesis of CNTs, included with an improvement of CNTs quality.

Piedigrosso et al. [11] reported that, CNTs are capable of catalytic hydrogenation, but there is no selective eliminate of solid carbon, either crystalline carbon or amorphous carbon. Catalytic hydrogenation may enhance the catalyst performance by removing the carbon covering the catalyst surface, which caused the deactivation of catalyst. In this work, an experiment was conducted to study the synthesis of CNTs in reduced-process, by comparing between processes with and without H_2 feed (R-woH$_2$ and R-wH$_2$) with a reaction time of 5 hours (300 min.) to study catalyst stability of both processes, as shown in Fig. 4.13.
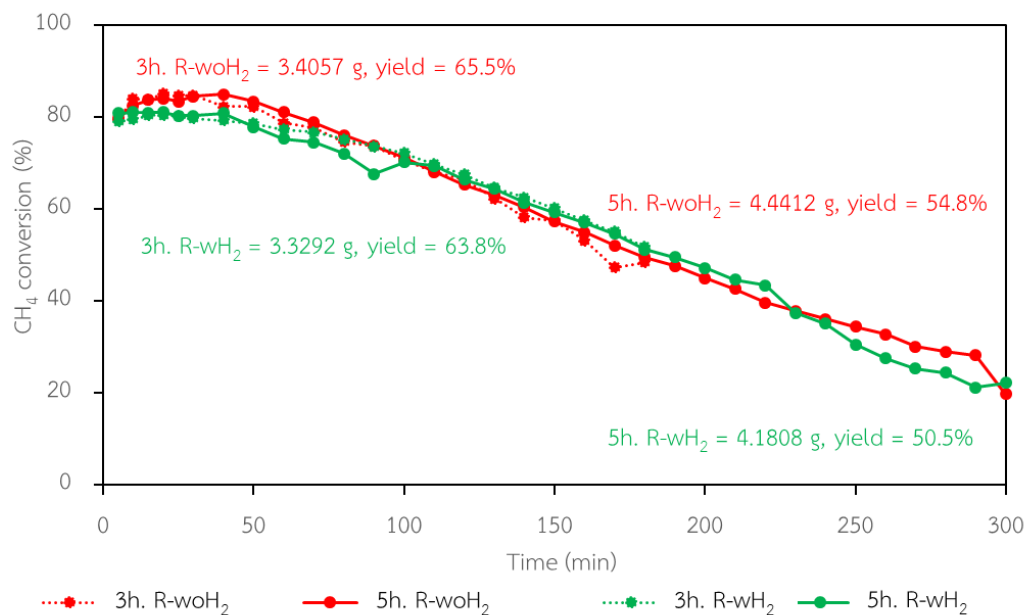
Figure 4. 13 CH_4 conversion over FeMo/MgO catalyst between R-woH$_2$ and R-wH$_2$
with reaction time 3h. (180 min) and 5h. (300 min)

Methane conversion of R-woH$_2$ and R-wH$_2$ process were shown in Fig 4.13, it can be seen that the conversion of methane continues to decrease at the same rate in both processes. Comparison the product weight difference between two processes, at 3 hours, the difference was about 0.07 g, but at 5 hours, the difference was about 0.26 g. Therefore, it seems that addition of H$_2$ does not keep catalyst stability, but also reduce the weight of the product.

The catalytic hydrogenation reaction was tested to prove these issues. As-prepared CNTs from R-woH$_2$ and R-wH$_2$ process were tested for catalytic hydrogenation reaction at 900°C with flow rates of 100 and 50 ml/min of H$_2$ and N$_2$, respectively. Effluent gas, product weight, and crystalline ratio were analyzed to identify the behavior that occurred.
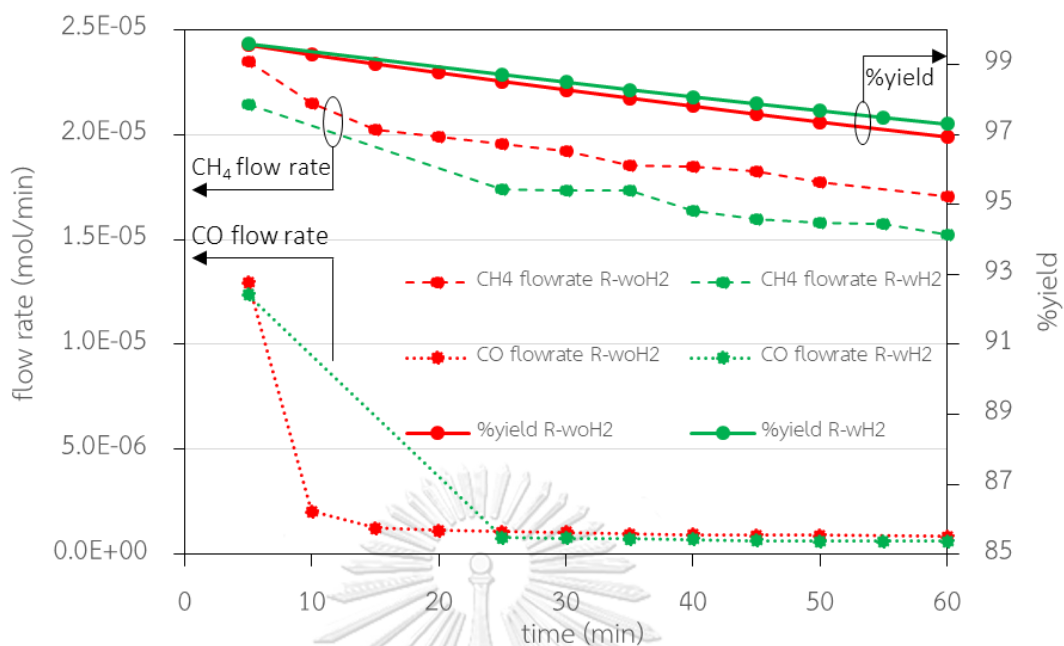
Figure 4. 14 Flow rate of CH$_4$ and CO, and %yield as a funtion of catalytic

hydrogenation reaction time

Figure 4.14 exhibited flow rate of CH$_4$ and CO released from the system during the catalytic hydrogenation reaction test. It also shows the calculated quantity of CNTs consumed as a %yield. From the experiment, it was found that CO was initially formed. Methane occurred throughout the experiment, with the flow rate decreasing slightly over time. After the experiment, approximately 3% of CNTs were consumed. In addition, CH$_4$ and CO generated rate have no different for each processes, although these two samples are expected to have different incidences, because R-wH$_2$ has been occurred in catalytic hydrogenation (during the formation of CNTs) for longer than R-woH$_2$. If the catalytic hydrogenation is a selective reaction, a difference will occur in some way.

The thermal stability of the product is shown in Fig 4.15, and the average crystallinity ratio by Raman characteristic is shown in Table 4.3
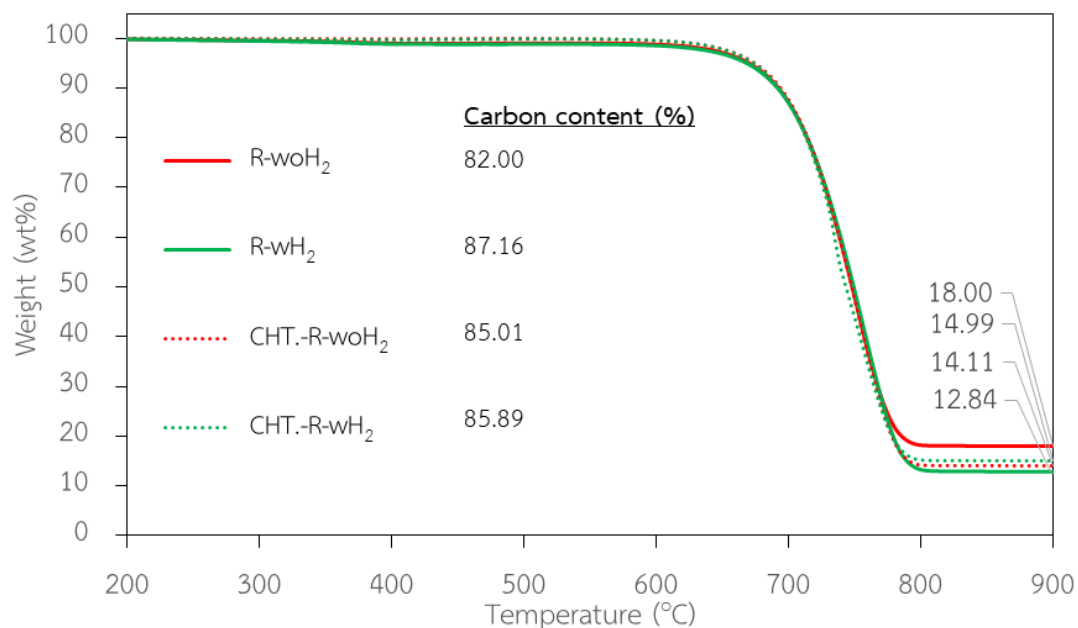
Figure 4. 15 TGA of CNTs for study of catalytic hydrogenation reaction.

Table 4. 3 Purity and average crystallinity ratio for study of catalytic hydrogenation reaction

Experimental	%purity (TGA)	Average I_G/I_D
R-woH$_2$	82.00	2.58±0.49
R-wH$_2$	87.16	2.56±0.24
Catalytic hydrogenation-R-woH$_2$	85.01	2.61±0.45
Catalytic hydrogenation-R-wH$_2$	85.89	2.60±0.14

From the thermal decomposition in Fig 4.15, it was found that all samples were not different, with similar carbon content and decomposed at the same temperature range. Consider the proportion of crystallinity. Raman analysis has shown no difference in I_G/I_D ratio with an average of 2.6

Therefore, from the study of the catalytic hydrogenation reaction. It can be concluded that the catalytic hydrogenation reaction occurs during the synthesis of CNTs where, as CNTs are used as a precursor to form methane and carbon monoxide. This reaction was not selective eliminate either crystalline or amorphous carbon. As a result, it does not improve the stability of the catalyst, by etching carbon from surface of catalyst. The addition of H_2 to the system will not enhance the properties of CNTs and produces less product, because of the catalytic hydrogenation reaction and the shifted of reaction equilibrium.

From the study of the role of H_2 in section 4.1, it was concluded that an important role of H_2 is to determine the catalyst structure by H_2 pre-reduction of catalyst before CNTs formation. Whereas the addition of H_2 during the formation of CNTs was not found to have a beneficial effect on the synthesis of CNTs and resulted in less product yield.

4.2 Kinetic study of CNTs synthesis

The aim of the kinetic study of CNTs synthesis was to investigate the mechanisms occurring during the synthesis of CNTs, with the hope that the data could be used for further process scale-up. Data collection for use in kinetic studies in CNTs synthesis is quite difficult because solids forming while reaction that made an unsteady state reaction. Researches have chosen a variety methods to investigated reaction rate, such as measuring the height of VACNTs [54], analysis of hydrogen output gas [55], or batch analysis by collect data on changing weight of the catalyst bed [52],[53]. In this work, batch analysis was used. The reaction rate in each process was collected as shown in Fig 4.16.
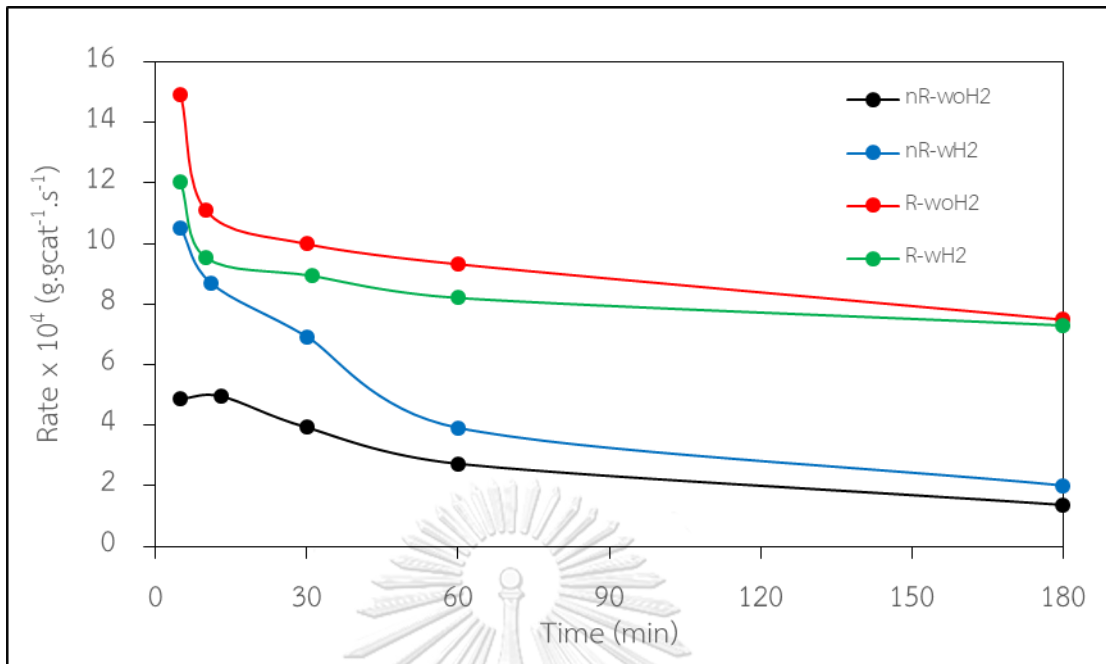
Figure 4. 16 yield rate of CNTs synthesis

The rate of product yield was calculated according to the equation (3.5), with units of gram product divided by grams of catalyst and reaction time in second. A dramatic decrease in yield rate can be observed in all processes. From the study in section 4.1 it was found that R-woH$_2$ process had the highest yield and was able to reduce the complexity of analysis by remove H$_2$ feeding. Therefore, this process was chosen for further kinetic studies with 30 minutes reaction time. The partial pressure of CH$_4$ in feed gas was varied to identify the reaction order and effects of CH$_4$ concentration.

The experimental data for kinetic study was shown in Table 4.4. Partial pressure of CH$_4$ was conducted by vary of CH$_4$ flow rate, product weight was measured then calculated to product yield and rate with equation (4.1) and (4.2), respectively.

$$\text{product yield (g)} = g_{product} - g_{reduced\text{-}catalyst} \text{ ; } g_{reduced\text{-}catalyst} = 0.75 \times g_{catalyst} \quad (4.1)$$

$$r_{CNTs}\left(g g_{cat.}^{-1} s^{-1}\right) = \frac{\text{product yield (g)}}{g_{reduced\text{-}catalyst} \times \text{reaction time (S)}} \quad (4.2)$$

Table 4. 4 Experimental data for kinetic study of CNTs formation

CH$_4$ flow rate (ml/min)	P$_{CH4}$	product weight (g)	product yield (g)	rate x10^4 (g.gcat^{-1}.s^{-1})
30	0.15	0.8178	0.4425	6.55
50	0.24	1.0490	0.6724	9.92
70	0.34	1.2690	0.8937	13.23
110	0.53	1.6903	1.3155	19.50
150	0.71	1.9255	1.5504	22.96
170	0.82	2.0924	1.7172	25.42
200	0.98	1.4853	1.1098	16.42

Effect of partial pressure of methane on rate of CNTs formation was found that the reaction rate changes according to the partial pressure of methane, as shown in Figure 4.17.
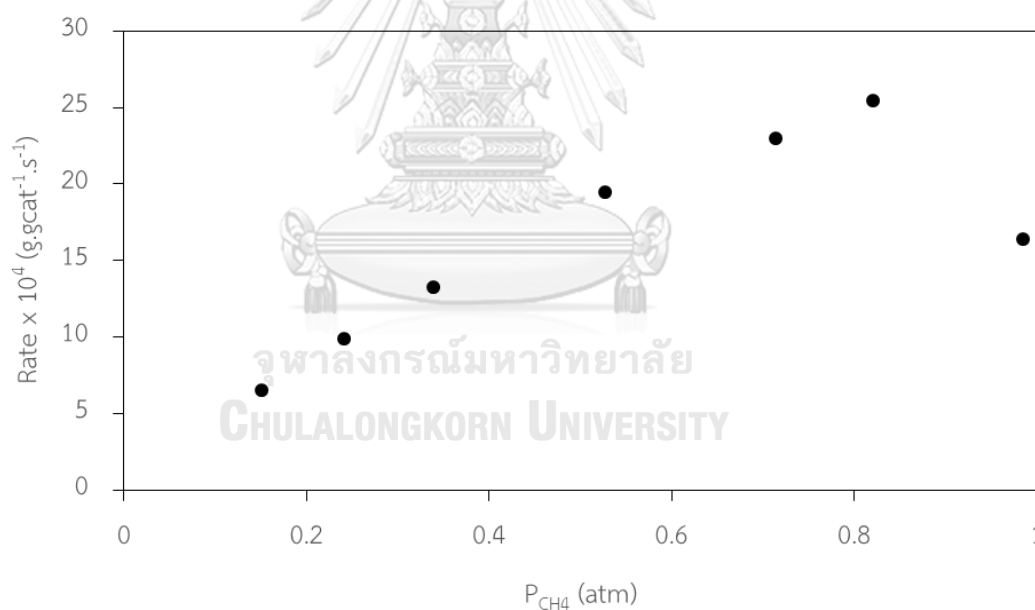
Figure 4. 17 Effect of partial pressure of methane on CNTs formation rate

Pseudo first order reaction kinetic was assumed to this reaction, lead to the following rate Eqs. (4.3). The rate constants are given by k$^{'}$. In order to estimate the

parameters k´, Eqs. (4.3) can be linearized and parameter was estimated from the slope as shown in Fig 4.18.

$$R = k^{'} P_{CH_4} \qquad\qquad (4.3)$$
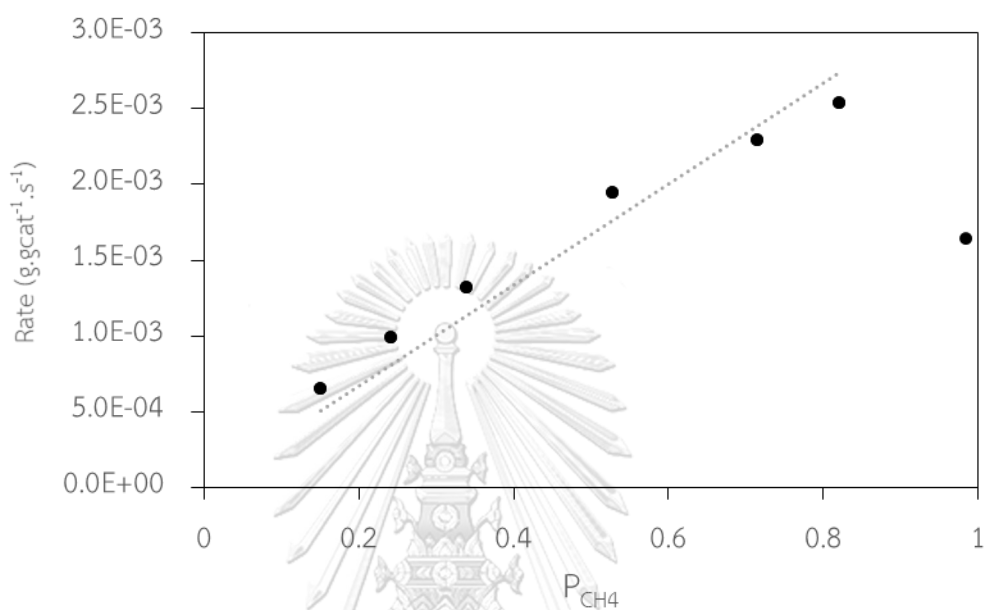
Figure 4. 18 Pseudo first order regression for methane decomposition

The linearization in Fig 4.18 not considered the partial pressure of methane equal to 1, as it is a pure methane system which is inconsistent with the other proportions. The value of the rate constant k´ is 0.033 ($gg_{cat}^{-1}s^{-1}atm^{-1}$).

The experimental and kinetic model were plotted as shown in Fig 4.19. It can be seen that kinetic model predicts the rate of decomposition of methane quite accurately. Kinetic model and experimental results can be observed that the rate of formation of CNTs increase with an increase in the partial pressure of methane, then reaches a saturation level followed by a decreased in the rate at higher partial pressures of methane.
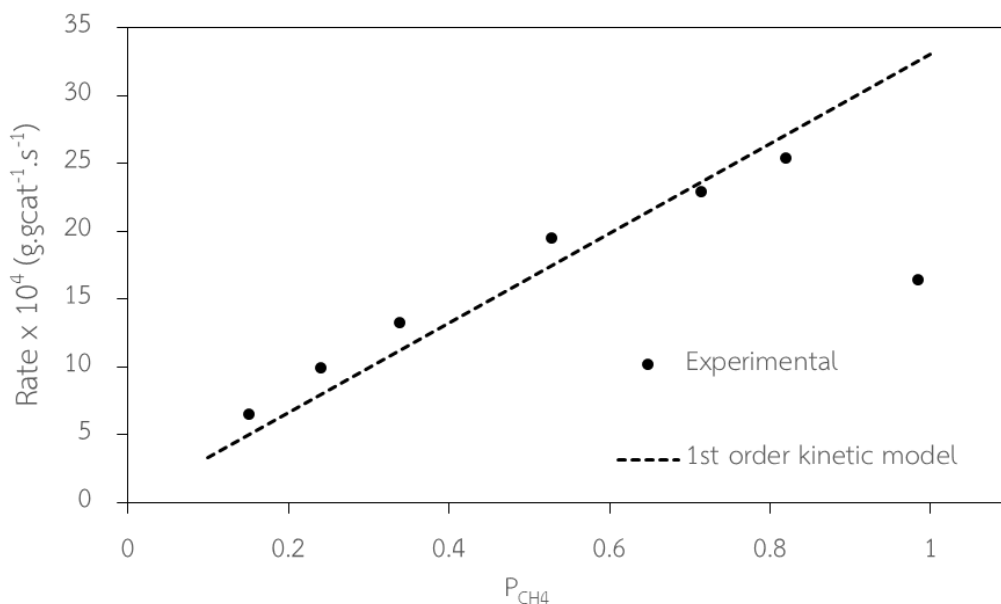
Figure 4. 19 pseudo 1st order for predicting the CNTs formation rate at 900°C

The effect of temperature was studied in the range of 850°C-1,000^{o}C with partial pressure of methane equal to 0.24 atm. (50ml/min). It was observed that the rate of CNTs formation increased with temperature until higher than 950°C because of catalyst begin to agglomerated that decreased catalyst performance, as shown in Fig 4.20.

To estimation of the activation energy (E$_a$), Arrhenius plot is needed. Then the rate of reaction (lnR$_{CNTs}$) was plotted vs. T^{-1} as shown in Fig 4.21. The rate of CNTs formation at 1,000^{o}C was not considered for E$_a$ estimation, as agglomerated of active phase occur.
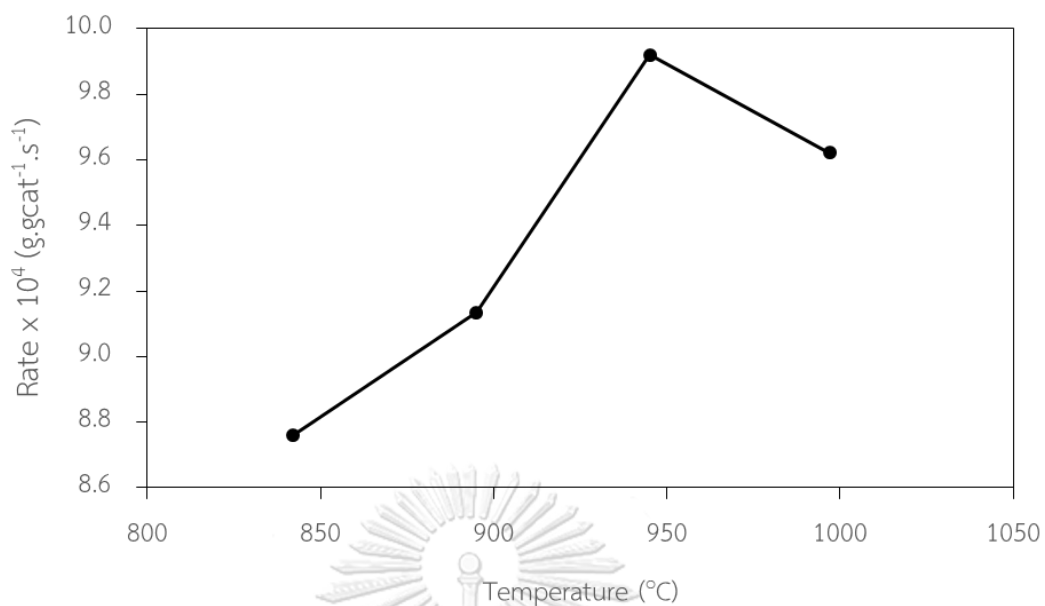
Figure 4. 20 Effect of temperature on CNTs formation rate
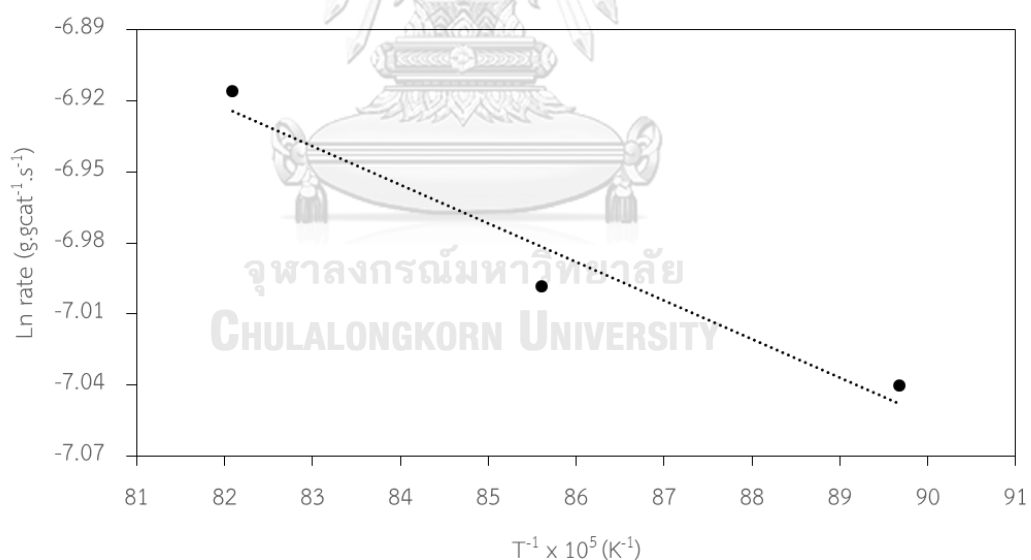
Figure 4. 21 Arrhenius plot for estimation of the activation energy

The activation energy was found to be 13.22 kJ mol^{-1}, compared to the other tasks in Table 2-2, our E$_a$ was much lower. It may be in a range of mass transfer limited [63], consistent with an assumption of pseudo first order reaction that used to

describe mass transfer limited the reaction rate. Additionally, our experiment found the behavior of the CNTs formation rapidly occur, and a compaction of the bed layer will occur, which may hinder the formation of CNTs, shows that this experimental process undesignated for study mass transfer limited the process, therefore it is possible that E_a has a lower value compared to other works. Moreover, E_a determinations should be carried out in reactions with low conversion and reaction temperatures to get accurate and reasonable values [64, 65]

Chapter 5

Conclusions and Suggestions

5.1 Conclusions

Synthesis of MWCNTs by CCVD from methane using FeMo/MgO as a catalyst can be operated under H_2 free conditions. In studying the roles of H_2, the effects of using H_2 and catalytic hydrogenation reactions, it was found that an important role of hydrogen in the synthesis of CNTs is to change the catalyst structure in the pre-reduction of catalyst processes. CNTs properties vary depending on the structure of the catalyst used. In FeMo/MgO catalyst system, non-reduced processes forms Mo_2C, which allows CNTs to be smaller in diameter and has a higher proportion of crystallinity than the process reduced-process. Reduced-process will form the metallic formation of FeMo, the result is getting higher yield more than 5 times.

The appropriate condition is pre-reduction of catalyst without H_2 feed during the CNTs formation, which have %yield, g-CNTs/g-catalyst, average diameter and crystallinity ratios of 67.77%, 5.77 g-CNTs/g-catalyst, 43.25 nm, and 2.58, respectively.

The addition of H_2 in non-reduced process increases productivity with an appropriate value, the more increased of H_2 the more equilibrium shifted, resulting in fewer CNTs.

The presence of H_2 during the formation of CNTs allows catalytic hydrogenation occurs. This reaction was not selective eliminate either crystalline or amorphous carbon. As a result, it does not improve the stability of the catalyst, by etching carbon from surface of the catalyst. This includes H_2 not enhancing the quality of CNTs by increasing the crystallinity ratio.

The kinetic model for CNTs synthesis, derived by pseudo first order reaction of methane decomposition, corresponded to this experiment. The formation rate of CNTs increases with an increase in the partial pressure of methane until reached saturation level, the formation rate will decrease. The activation energy was found to be 13.22 $kJ\ mol^{-1}$, making the rate-controlling step likely to be in the range of mass transfer controlled.

5.2 Suggestions

1.   Develop a more uniform catalyst to reduce distributed data.

2.   Further study in mono-metallic catalysts such as Fe or Mo.

3.   The effect of H_2 concentrations on the R-wH$_2$ system should be studied to confirm the induced behavior.

4.   Kinetic study by considering other factors affecting the process such as flow rate, bed height, bed length, and catalyst loading.

5.   Test the catalytic hydrogenation reaction under other conditions such as changes in temperature, time, and test samples.

6.   Additional catalyst stability tests on other systems to verify that deactivated of the system caused by the catalyst or not.

7.   The process of determining the structure of the catalyst (metallic/carbide) should be studied to selective synthesis of CNTs.

REFERENCES

[1] Iijima S. Helical microtubules of graphitic carbon. nature. 1991;354:56-8.

[2] Cheptubes. Carbon Nanotubes Properties and Applications. cheaptubes: cheaptubes.

[3] Torres D, Pinilla J, Lázaro M, Moliner R, Suelves I. Hydrogen and multiwall carbon nanotubes production by catalytic decomposition of methane: Thermogravimetric analysis and scaling-up of Fe–Mo catalysts. International journal of hydrogen energy. 2014;39:3698-709.

[4] Łamacz A. CNT and H2 Production During CH4 Decomposition over Ni/CeZrO2. I. A Mechanistic Study. ChemEngineering. 2019;3:26.

[5] Fan Z, Weng W, Zhou J, Gu D, Xiao W. Catalytic decomposition of methane to produce hydrogen: A review. Journal of Energy Chemistry. 2020;58:415-30.

[6] Torres D, Pinilla JL, Suelves I. Cobalt doping of α-Fe/Al2O3 catalysts for the production of hydrogen and high-quality carbon nanotubes by thermal decomposition of methane. International Journal of Hydrogen Energy. 2020;45:19313-23.

[7] Wang H, Yang L, Sui X, Karahan HE, Wang X, Chen Y. Selective synthesis of single walled carbon nanotubes on metal (iron, nickel or cobalt) sulfate-based catalysts. Carbon. 2018;129:128-36.

[8] Abdullahi I, Sakulchaicharoen N, Herrera JE. Selective synthesis of single-walled carbon nanotubes on Fe–MgO catalyst by chemical vapor deposition of methane. Diamond and Related Materials. 2014;41:84-93.

[9] Chang K-h, Kim J-d, Yoon K-w. Continuous manufacturing apparatus and method for carbon nanotubes having gas separation units. Google Patents; 2018.

[10] Inoue S, Lojindarat S, Kawamoto T, Matsumura Y, Charinpanitkul T. Spontaneous and controlled-diameter synthesis of single-walled and few-walled carbon nanotubes. Chemical Physics Letters. 2018;699:88-92.

[11] Piedigrosso P, Colomer JF, Fonseca A, Nagy JB. Effect of hydrogenation on catalytically produced carbon nanotubes. AIP Conference Proceedings1998. p. 16-9.

[12] Pinheiro P, Schouler M, Gadelle P, Mermoux M, Dooryhee E. Effect of hydrogen on the orientation of carbon layers in deposits from the carbon monoxide disproportionation reaction over Co/Al2O3 catalysts. Carbon. 2000;38:1469-79.

[13] Xiong GY, Suda Y, Wang DZ, Huang JY, Ren ZF. Effect of temperature, pressure, and gas ratio of methane to hydrogen on the synthesis of double-walled carbon nanotubes by chemical vapour deposition. Nanotechnology. 2005;16:532-5.

[14] Biris AR, Li Z, Dervishi E, Lupu D, Xu Y, Saini V, et al. Effect of hydrogen on the growth and morphology of single wall carbon nanotubes synthesized on a FeMo/MgO catalytic system. Physics Letters A. 2008;372:3051-7.

[15] Behr MJ, Gaulding EA, Mkhoyan KA, Aydil ES. Effect of hydrogen on catalyst nanoparticles in carbon nanotube growth. Journal of Applied Physics. 2010;108.

[16] Reynolds C, Duong B, Seraphin S. Effects of hydrogen flow rate on carbon nanotube growth. J Undergraduate Res Phys. 2010.

[17] Schünemann C, Schäffel F, Bachmatiuk A, Queitsch U, Sparing M, Rellinghaus B, et al. Catalyst poisoning by amorphous carbon during carbon nanotube growth: fact or fiction? ACS nano. 2011;5:8928-34.

[18] Li Y, Ji K, Duan Y, Meng G, Dai Z. Effect of Hydrogen Concentration on the Growth of Carbon Nanotube Arrays for Gecko-Inspired Adhesive Applications. Coatings. 2017;7.

[19] Hao Y, Qingwen L, Jin Z, Zhongfan L. The effect of hydrogen on the formation of nitrogen-doped carbon nanotubes via catalytic pyrolysis of acetonitrile. Chemical Physics Letters. 2003;380:347-51.

[20] Lamouroux E, Serp P, Kihn Y, Kalck P. Identification of key parameters for the selective growth of single or double wall carbon nanotubes on FeMo/Al2O3 CVD catalysts. Applied Catalysis A: General. 2007;323:162-73.

[21] Hart AJ, Slocum AH, Royer L. Growth of conformal single-walled carbon nanotube films from Mo/Fe/Al2O3 deposited by electron beam evaporation. Carbon. 2006;44:348-59.

[22] Chung UC, Lee DB, Jeong YU, Ha MJ, Chung WS. Effect of H_2 Gas on Carbon Nanotubes Synthesis. Materials Science Forum. 2005;475-479:3559-62.

[23] He Z, Maurice J-L, Gohier A, Lee CS, Pribat D, Cojocaru CS. Iron Catalysts for the Growth of Carbon Nanofibers: Fe, Fe3C or Both? Chemistry of Materials. 2011;23:5379-87.

[24] Emmenegger C, Bonard J-M, Mauron P, Sudan P, Lepora A, Grobety B, et al. Synthesis of carbon nanotubes over Fe catalyst on aluminium and suggested growth mechanism. Carbon. 2003;41:539-47.

[25] Kalaichelvan K. Synthesis of carbon nanotubes using Fe-Mo/Al 2 O 3 bimetallic catalyst by CVD method. IEEE-International Conference On Advances In Engineering, Science And Management (ICAESM-2012): IEEE; 2012. p. 429-33.

[26] Markets Ra. The Global Carbon Nanotubes (CNT) Market (2018-2023) is Projected to Grow at a CAGR of 16.7% - Technological Advancements and Decreasing Production Cost is Driving Growth. PRNewswire: PRNewswire; 2018.

[27] Sigma-Aldrich. 755710 Sigma-Aldrich Carbon nanotube, single-walled >70% (TGA). sigmaaldrich: sigmaaldrich.

[28] Sigma-Aldrich. 755133 Sigma-Aldrich Carbon nanotube, multi-walled thin, <5% Metal Oxide(TGA). sigmaaldrich: sigmaaldrich.

[29] ResearchAndMarkets. Global Carbon Nanotubes Market Report 2020: Production Capacities for MWCNTS and SWCNTs, Historical and Forecast to 2030 - ResearchAndMarkets.com. Businesswire: Businesswire; 2020.

[30] Berger M. Carbon nanotubes – what they are, how they are made, what they are used for. Nanowerk: Nanowerk.

[31] Rafique MMA, Iqbal J. Production of carbon nanotubes by different routes-a review. Journal of encapsulation and adsorption sciences. 2011;1:29.

[32] Shah KA, Tali BA. Synthesis of carbon nanotubes by catalytic chemical vapour deposition: A review on carbon sources, catalysts and substrates. Materials Science in Semiconductor Processing. 2016;41:67-82.

[33] Yadav MD, Dasgupta K, Patwardhan AW, Kaushal A, Joshi JB. Kinetic study of single-walled carbon nanotube synthesis by thermocatalytic decomposition of methane using floating catalyst chemical vapour deposition. Chemical Engineering Science. 2019;196:91-103.

[34] Jafarpour SM, Kini M, Schulz SE, Hermann S. Effects of catalyst configurations and process conditions on the formation of catalyst nanoparticles and growth of single-walled carbon nanotubes. Microelectronic Engineering. 2017;167:95-104.

[35] Rümmeli MH, Bachmatiuk A, Börrnert F, Schäffel F, Ibrahim I, Cendrowski K, et al. Synthesis of carbon nanotubes with and without catalyst particles. Nanoscale research letters. 2011;6:1-9.

[36] Moisala A, Nasibulin AG, Kauppinen EI. The role of metal nanoparticles in the catalytic production of single-walled carbon nanotubes—a review. Journal of Physics: condensed matter. 2003;15:S3011.

[37] Liu W-W, Aziz A, Chai S-P, Mohamed AR, Hashim U. Synthesis of single-walled carbon nanotubes: Effects of active metals, catalyst supports, and metal loading percentage. Journal of Nanomaterials. 2013;2013.

[38] Awadallah AE, Abdel-Hamid SM, El-Desouki DS, Aboul-Enein AA, Aboul-Gheit AK. Synthesis of carbon nanotubes by CCVD of natural gas using hydrotreating catalysts. Egyptian Journal of Petroleum. 2012;21:101-7.

[39] Xu X, Huang S, Yang Z, Zou C, Jiang J, Shang Z. Controllable synthesis of carbon nanotubes by changing the Mo content in bimetallic Fe–Mo/MgO catalyst. Materials Chemistry and Physics. 2011;127:379-84.

[40] Li Y, Kim W, Zhang Y, Rolandi M, Wang D, Dai H. Growth of single-walled carbon nanotubes from discrete catalytic nanoparticles of various sizes. The Journal of Physical Chemistry B. 2001;105:11424-31.

[41] Li Y, Liu J, Wang Y, Wang ZL. Preparation of monodispersed Fe– Mo nanoparticles as the catalyst for CVD synthesis of carbon nanotubes. Chemistry of Materials. 2001;13:1008-14.

[42] Cheung CL, Kurtz A, Park H, Lieber CM. Diameter-controlled synthesis of carbon nanotubes. The Journal of Physical Chemistry B. 2002;106:2429-33.

[43] Awadallah AE, Aboul-Enein AA. Catalytic decomposition of methane to COx-free hydrogen and carbon nanotubes over Co–W/MgO catalysts. Egyptian Journal of Petroleum. 2015;24:299-306.

[44] Ashik U, Daud WW, Hayashi J-i. A review on methane transformation to hydrogen and nanocarbon: relevance of catalyst characteristics and experimental parameters on yield. Renewable and Sustainable Energy Reviews. 2017;76:743-67.

[45] Łamacz A, Łabojko G. CNT and H2 production during CH4 decomposition over Ni/CeZrO2. II. Catalyst performance and its regeneration in a fluidized bed. ChemEngineering. 2019;3:25.

[46] Liu Q, Wu P, He J, Liu C, Jiang W. Catalytic decomposition of methane by two-step cascade catalytic process: Simultaneous production of hydrogen and carbon nanotubes. Chemical Engineering Research and Design. 2020;163:96-106.

[47] Qian JX, Chen TW, Enakonda LR, Liu DB, Basset J-M, Zhou L. Methane decomposition to pure hydrogen and carbon nano materials: State-of-the-art and future perspectives. International Journal of Hydrogen Energy. 2020.

[48] Wang H, Gu G, Zhu S, Yang L, Chen Y. Synthesis of (9, 8) single-walled carbon nanotubes on CoSO4/SiO2 catalysts: The effect of Co mass loadings. Carbon. 2020;169:288-96.

[49] Yadav MD, Patwardhan AW, Joshi JB, Dasgupta K. Selective synthesis of metallic and semi-conducting single-walled carbon nanotube by floating catalyst chemical vapour deposition. Diamond and Related Materials. 2019;97:107432.

[50] Chung UC, Lee DB, Jeong Y, Ha M, Chung WS. Effect of H2 Gas on Carbon Nanotubes Synthesis. Materials Science Forum: Trans Tech Publ; 2005. p. 3559-62.

[51] Robertson J. Heterogeneous catalysis model of growth mechanisms of carbon nanotubes, graphene and silicon nanowires. Journal of Materials Chemistry. 2012;22:19858-62.

[52] Ni L, Kuroda K, Zhou L-P, Kizuka T, Ohta K, Matsuishi K, et al. Kinetic study of carbon nanotube synthesis over Mo/Co/MgO catalysts. Carbon. 2006;44:2265-72.

[53] Hsieh C-T, Lin Y-T, Chen W-Y, Wei J-L. Parameter setting on growth of carbon nanotubes over transition metal/alumina catalysts in a fluidized bed reactor. Powder Technology. 2009;192:16-22.

[54] Wirth CT, Zhang C, Zhong G, Hofmann S, Robertson J. Diffusion-and reaction-limited growth of carbon nanotube forests. ACS nano. 2009;3:3560-6.

[55] Pirard SL, Douven S, Bossuot C, Heyen G, Pirard J-P. A kinetic study of multi-walled carbon nanotube synthesis by catalytic chemical vapor deposition using a Fe–Co/Al2O3 catalyst. Carbon. 2007;45:1167-75.

[56] Douven S, Pirard SL, Heyen G, Toye D, Pirard J-P. Kinetic study of double-walled carbon nanotube synthesis by catalytic chemical vapour deposition over an Fe-Mo/MgO catalyst using methane as the carbon source. Chemical engineering journal. 2011;175:396-407.

[57] Tan S, Ojovan MI, Hyatt NC, Hand RJ. MoO3 incorporation in magnesium aluminosilicate glasses. Journal of Nuclear Materials. 2015;458:335-42.

[58] Fellicia D, Sutarsis, Kurniawan B, Wulanari D, Purniawan A, Wibisono T. Study of Sigma Phase in Duplex SAF 2507. IOP Conference Series: Materials Science and Engineering. 2017;202:012039.

[59] Das R, Bee Abd Hamid S, Eaqub Ali M, Ramakrishna S, Yongzhi W. Carbon nanotubes characterization by X-ray powder diffraction–a review. Current Nanoscience. 2015;11:23-35.

[60] Duc Vu Quyen N, Quang Khieu D, Tuyen TN, Xuan Tin D, Thi Hoang Diem B. Carbon nanotubes: Synthesis via chemical vapour deposition without hydrogen, surface modification, and application. Journal of Chemistry. 2019;2019.

[61] Kashiwaya Y, Watanabe M. Kinetic analysis of the decomposition reaction of CH4 injecting into molten slag. ISIJ international. 2012;52:1394-403.

[62] Wang J, Jin L, Yu G, Hu H. Effect of hydrogen addition on formation of hydrogen and carbon from methane decomposition over Ni/Al2O3. The Canadian Journal of Chemical Engineering. 2020;98:536-43.

[63] Fogler HS. Essentials of Chemical Reaction Engineering: Essenti Chemica Reactio Engi: Pearson Education; 2010.

[64] Bartholomew CH, Farrauto RJ. Fundamentals of industrial catalytic processes: John Wiley & Sons; 2011.

[65] Hartmann M, Machoke AG, Schwieger W. Catalytic test reactions for the evaluation of hierarchical zeolites. Chemical Society Reviews. 2016;45:3313-30.

จุฬาลงกรณ์มหาวิทยาลัย
CHULALONGKORN UNIVERSITY

APPENDIX

Appendix A

Calculations

A.1 Conversion

For reactions in chemical processes, the reactants which are fed into the system are partially reacted. The conversion is the ratio between reacted reactant with the total reactant in feed stream. The effluent gas was collected and analyzed with Gas Chromatography (GC-TCD 8A, Shimadzu). The gas content of methane, carbon monoxide and nitrogen were calculated from by Eq. (A.1), (A.2), and (A.3) the calibration curve as shown in Figure A.1-A.3, respectively.

$$y = 49,080,169,087.62x \tag{A.1}$$

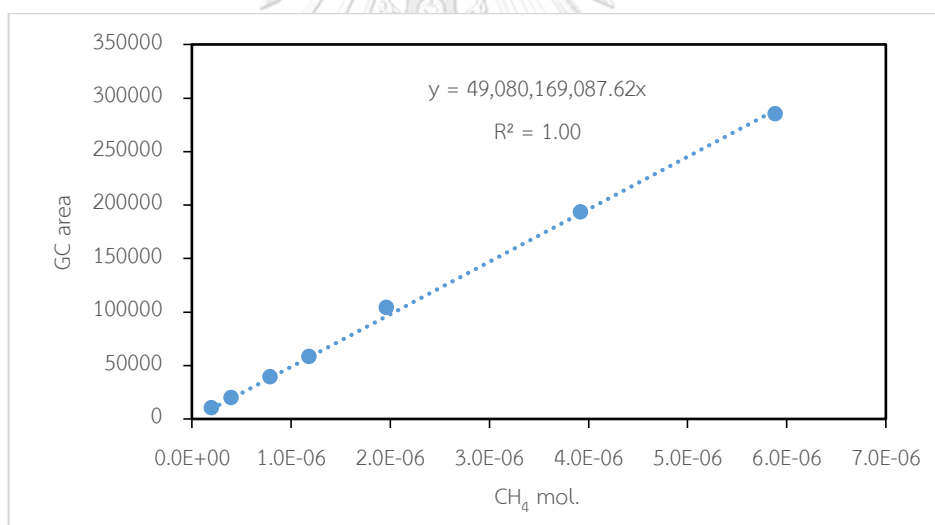Where y is the graph area from GC and x is mol of CH_4 in sample 0.25ml

Figure A. 1 CH_4 calibration curve

$$y = 88,338,898,695.99x \tag{A.2}$$

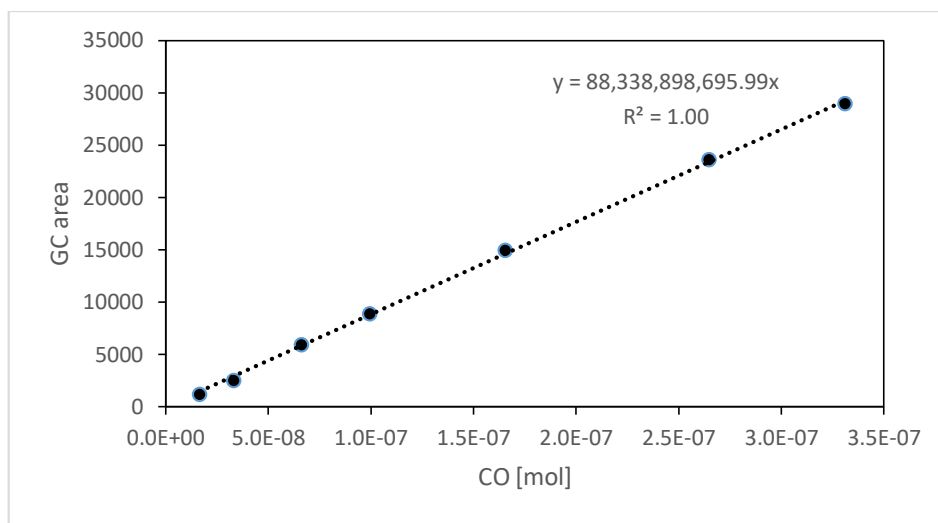Where y is the graph area from GC and x is mol of CO in sample 0.25ml

Figure A. 2 CO calibration curve

$$y= 54,392,950,417.18x \tag{A.3}$$

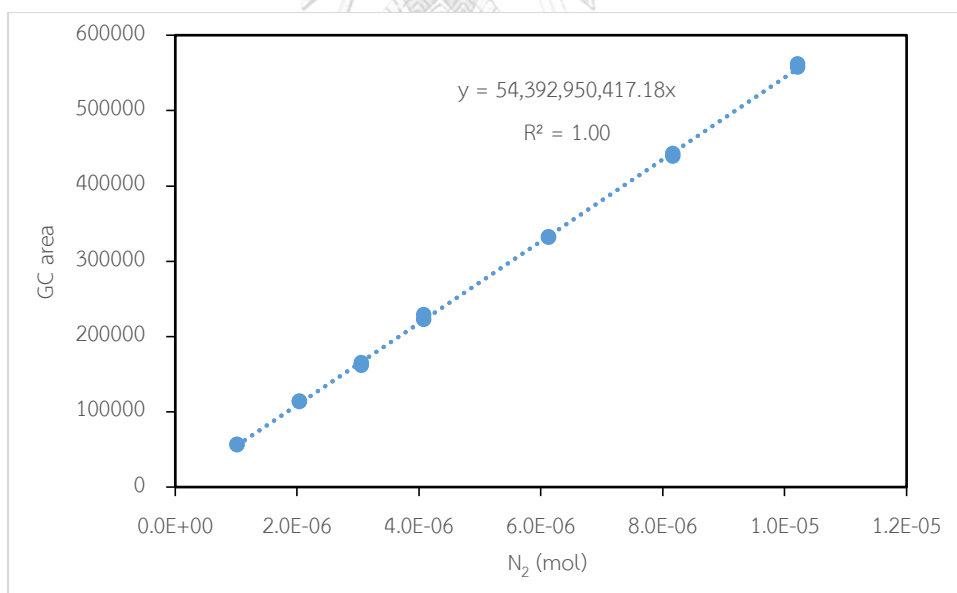Where y is the graph area from GC and x is mol of N_2 in sample 0.25ml

Figure A. 3 N_2 calibration curve

Methane conversion was calculated by Eq. (A.4)

$$CH_4 \text{ conversion} = \frac{\text{Amount of } CH_4 \text{consumed}}{\text{Amount of } CH_4 \text{ in feed steam}} \times 100\% \tag{A.4}$$

Example of CH_4 conversion calculation was exhibited following Eq.(A.4). Addition information shown in Table A.1

Table A. 1 calculation of CH_4 conversion

Reaction time	Flow rate (ml/min)	mol CH_4 in sample 0.25 ml	CH_4 flow rate x0.25	CH_4 conversion
CH_4 at 10 min	337	1.48E-06	1.99E-03	69.27
CH_4 (feed stream)	200	8.09E-06	6.47E-03	

Using Eq. (A.4)

Methane conversion $= \dfrac{0.00647 - 0.00199 \text{ molCH}_4}{0.00647 \text{ mol CH}_4} \times 100\%$

$= 69.27\%$

A.2 carbon yield and g-CNTs/g-catalyst

Carbon yield was measured the weight of product deduct with the weight of catalyst used divided by carbon feed (g) as shown in Eq. (A.5). g-CNTs/g-catalyst was used to reported number of products per catalyst weight as shown in Eq. (A.6)

Carbon yield $= \dfrac{\text{product weight (g)- catalyst weight (g)}}{\text{total carbon fed into system (g)}} \times 100\%$ (A.5)

g-CNTs/g-catalyst $= \dfrac{\text{product weight (g)- catalyst weight (g)}}{\text{catalyst weight (g)}} \times 100\%$ (A.6)

A.3 Kinetic study

A.3.1 yield rate of CNTs formation
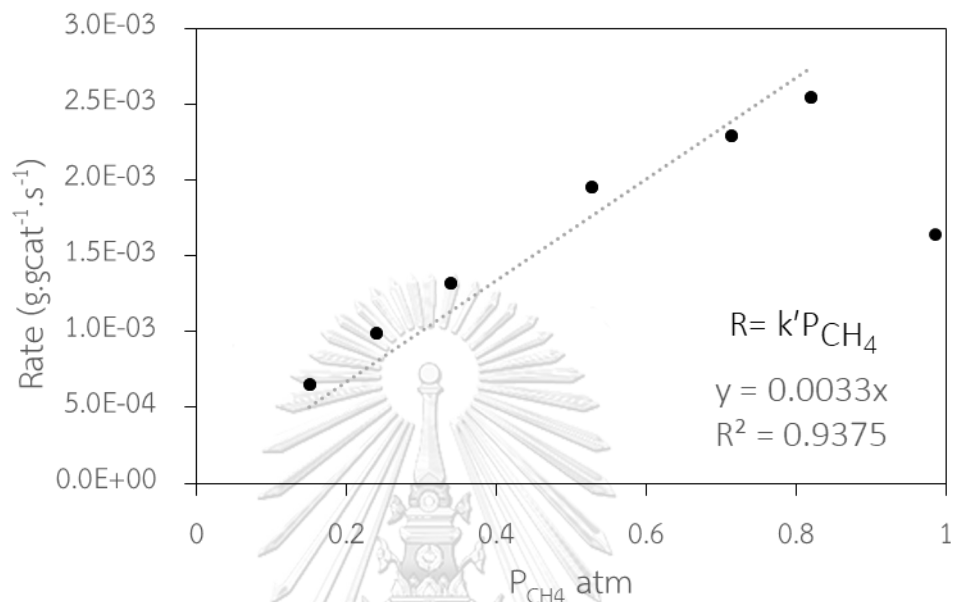
Yield rate was calculated according to the equation (A.7).

r_{CNTs} (g.gcat^{-1}.s^{-1}) $= \dfrac{\text{product weight (g)-reduced catalyst weight(g)}}{\text{reduced catalyst weight(g)} \times \text{reaction time (s)}}$ (A.7)
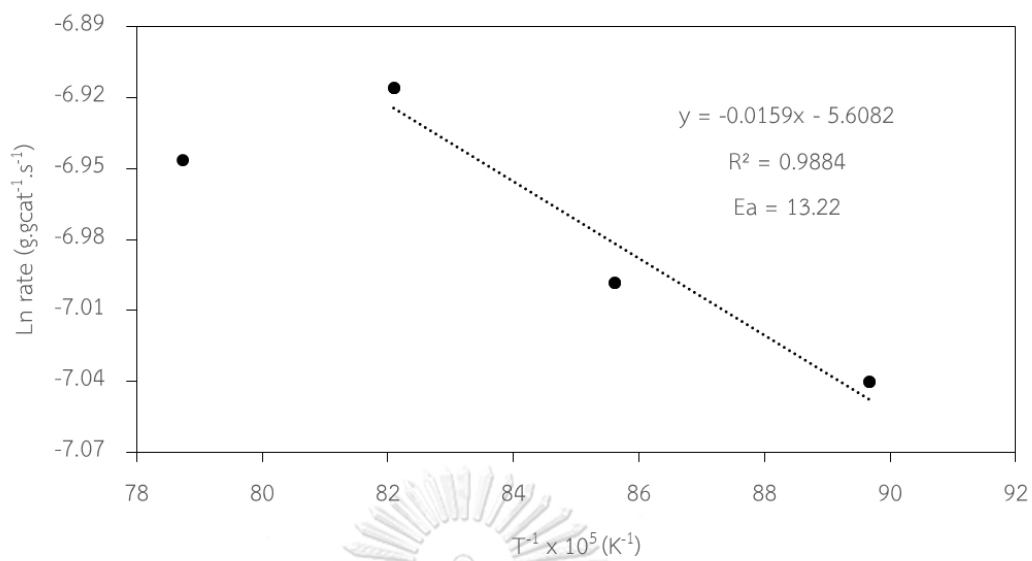
A.3.2 kinetic parameter estimation

Rate constant k' estimated from linearization as shown in Fig A.4 and calculated with Eq. (A.8).

Figure A. 4 Linearization to estimated rate constant k'

$$k'(gg_{cat}^{-1}s^{-1}atm^{-1})= slope =0.0033 \tag{A.8}$$

The activation energy was estimated through Arrhenius plot between Ln rate vs. T^{-1} as shown in Fig A.5 and calculated with Eq. (A.9)

Figure A. 5 Arrhenius plot for estimation of the activation energy

E_a = slope x ideal gas constant

= 0.0159x8.314 J mol^{-1}k^{-1} x 10^5/10^3 = 13.22 kJ mol^{-1}

จุฬาลงกรณ์มหาวิทยาลัย

CHULALONGKORN UNIVERSITY

Appendix B

Addition information

B.1 TEM images of as-prepared CNTs

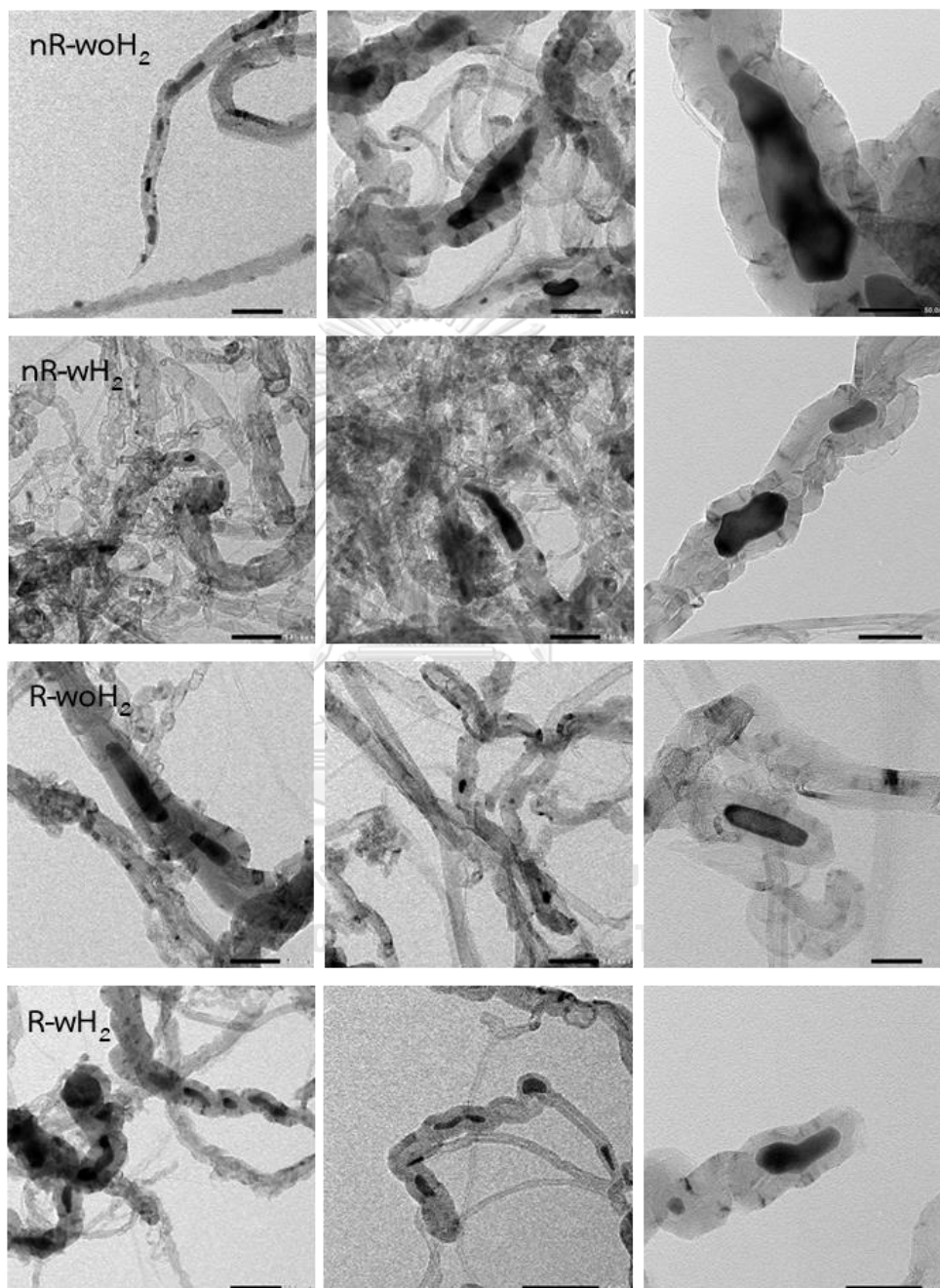**Figure A. 6** TEM images of as-prepared CNTs
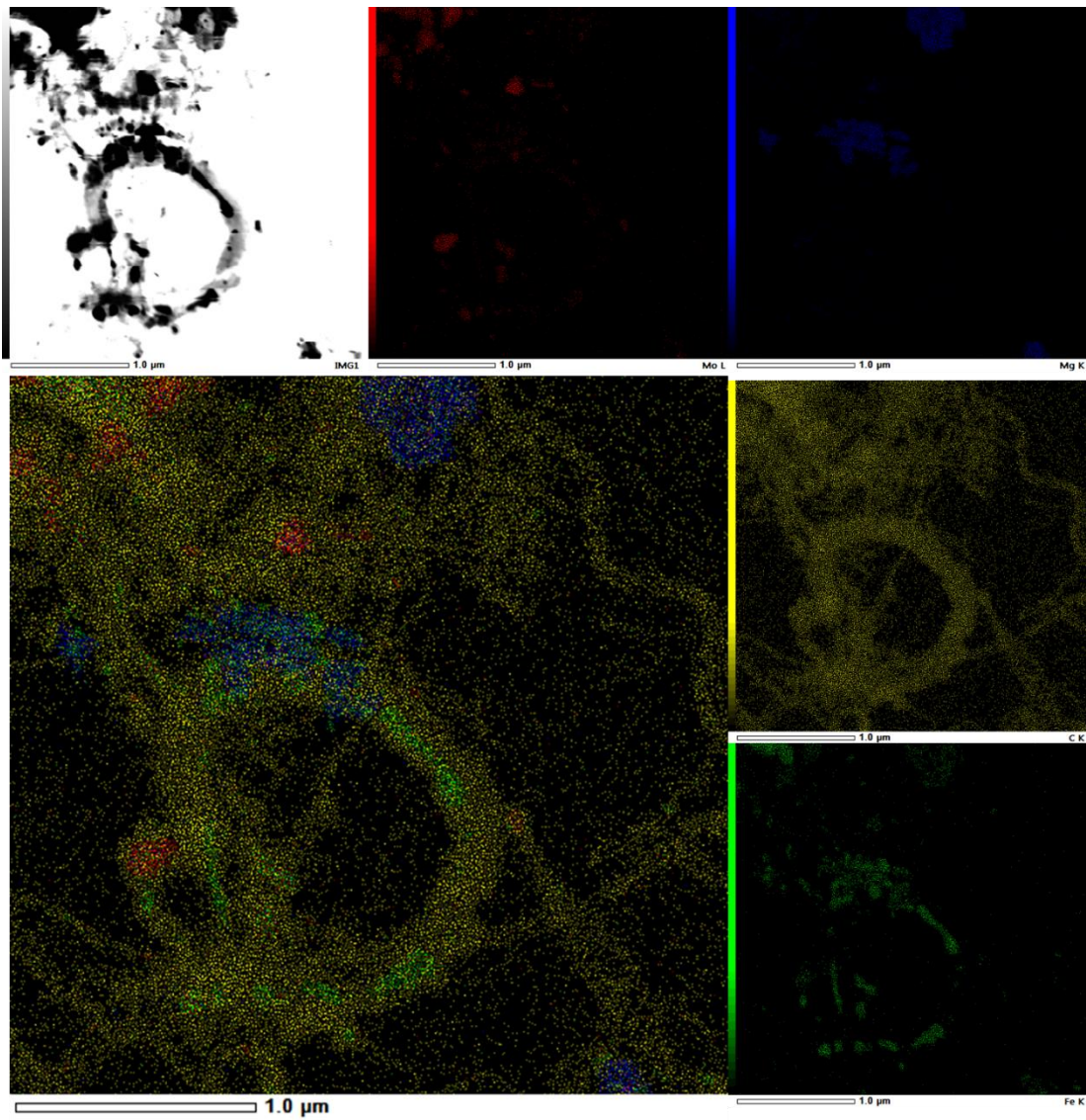
B.2 Element mapping of as-prepared CNTs

Figure A. 7 element mapping of as-prepared CNTs

VITA

NAME	Chawalkul Chotmunkhongsin
DATE OF BIRTH	09 march 1997
PLACE OF BIRTH	Bangkok Thailand
INSTITUTIONS ATTENDED	Chemical engineering mahidol university
HOME ADDRESS	59/2-5 Nongkhaem, Bangkok 10160